Improved methods for Feynman path integral calculations and their application to calculate converged vibrational–rotational partition functions, free energies, enthalpies, entropies, and heat capacities for methane

Steven L. Mielke and Donald G. Truhlar

Citation: The Journal of Chemical Physics **142**, 044105 (2015); doi: 10.1063/1.4905526
View online: http://dx.doi.org/10.1063/1.4905526
View Table of Contents: http://scitation.aip.org/content/aip/journal/jcp/142/4?ver=pdfcov
Published by the AIP Publishing

Improved methods for Feynman path integral calculations and their application to calculate converged vibrational–rotational partition functions, free energies, enthalpies, entropies, and heat capacities for methane

Steven L. Mielke[a] and Donald G. Truhlar[a]
Department of Chemistry, Chemical Theory Center, and Supercomputing Institute, University of Minnesota, 207 Pleasant St. S.E., Minneapolis, Minnesota 55455-0431, USA

(Received 20 November 2014; accepted 19 December 2014; published online 23 January 2015)

We present an improved version of our "path-by-path" enhanced same path extrapolation scheme for Feynman path integral (FPI) calculations that permits rapid convergence with discretization errors ranging from $O(P^{-6})$ to $O(P^{-12})$, where P is the number of path discretization points. We also present two extensions of our importance sampling and stratified sampling schemes for calculating vibrational–rotational partition functions by the FPI method. The first is the use of importance functions for dihedral angles between sets of generalized Jacobi coordinate vectors. The second is an extension of our stratification scheme to allow some strata to be defined based only on coordinate information while other strata are defined based on both the geometry and the energy of the centroid of the Feynman path. These enhanced methods are applied to calculate converged partition functions by FPI methods, and these results are compared to ones obtained earlier by vibrational configuration interaction (VCI) calculations, both calculations being for the Jordan–Gilbert potential energy surface. The earlier VCI calculations are found to agree well (within ~1.5%) with the new benchmarks. The FPI partition functions presented here are estimated to be converged to within a 2σ statistical uncertainty of between 0.04% and 0.07% for the given potential energy surface for temperatures in the range 300–3000 K and are the most accurately converged partition functions for a given potential energy surface for any molecule with five or more atoms. We also tabulate free energies, enthalpies, entropies, and heat capacities. © *2015 AIP Publishing LLC.* [http://dx.doi.org/10.1063/1.4905526]

I. INTRODUCTION

The textbook[1] route to the calculation of molecular conformational–vibrational–rotational partition functions involves the summation of Boltzmann factors. However, unless further approximations are invoked, this approach is limited to very small system sizes because it requires a complete set of vibrational–rotational eigenvalues up to reasonably high energies. One of the largest systems thus far treated in this manner is CH_4, where Chakraborty *et al.*[2] employed vibrational configuration interaction (VCI),[2–15] together with a multimode approximation,[9,16] to obtain eigenvalues for the Jordan–Gilbert (JG) potential energy surface (PES)[17] for total angular momenta in the range $J = 0$–50. One of the goals of the present paper is to compute very well converged partition functions by Feynman path integral methods[18–25] for the same PES and to use them to assess the accuracy of these VCI calculations.

We note that the JG PES is not the most accurate available PES; most recent studies[7,14,26–29] of the eigenspectrum of CH_4 have used the more accurate T8 PES of Schwenke and Partridge.[30] The JG PES was instead chosen by Chakraborty *et al.* because of the availability of literature values for comparison, in particular, due to its use in the first accurate quantum mechanical (QM) treatment[31,32] of the thermal rate constant for a reaction with more than four atoms, namely, the $H + CH_4 \rightarrow H_2 + CH_3$ reaction. In this work, Bowman *et al.*[32] showed that the initially reported QM rate constants,[31] which disagreed with variational transition state theory (VTST) calculations,[33] were inaccurate because the QM dynamics treatment was paired with a harmonic treatment of the reactant partition functions (when an anharmonic treatment of the partition functions was considered the QM and earlier VTST results were in good agreement). These treatments[31,32] only explicitly considered $J = 0$ and invoked a separable rotation or J-shifting approximation[34–39] to predict what the J-summed results would be. Testing the validity of this J-shifting approximation for the CH_4 partition functions was one goal of the work of Chakraborty *et al.*

Feynman path integral methods, together with Monte Carlo sampling, provide a means for calculating partition functions for systems that are too large to treat by summing Boltzmann factors. One goal of the work presented in this article is to introduce a number of numerical improvements made to our previous path integral methods.[40–50] In particular, we have generalized our importance sampling method to include dihedral angles (as in torsions, but more generally), we have generalized our stratified sampling scheme so that some strata may now be defined by geometric considerations while others are defined by energy considerations, and we have improved our extrapolation approach so that we can make use of expressions for which the errors scale as $O(P^{-n})$ for $n = 6, 8, 10$, or 12 and where P is the number of discretization points used to define the Feynman paths. A second goal, as

[a]Electronic addresses: slmielke@gmail.com and truhlar@umn.edu

stated above, is to obtain a set of benchmark calculations on the JG PES to compare to the earlier VCI-calculated partition functions.

The rest of this article is organized as follows. In Sec. II, we discuss the background needed to understand the algorithms, and we present the numerical enhancements. In Sec. III, we present path integral results for CH_4; in Sec. IV, we discuss the results and compare the path integral result to the earlier VCI results; and in Sec. V, we give concluding remarks.

II. BACKGROUND AND THEORY

A. Basic algorithm

The conformational-vibrational-rotational partition function, Q, may be expressed as

$$Q = \frac{1}{\sigma_{\rm sym}} \int_{-\infty}^{\infty} d\mathbf{x}\, \rho(\mathbf{x},T), \tag{1}$$

where T is the temperature, $\mathbf{x}$ is an N-dimensional configuration space point (with the center-of-mass motion removed so that N is $3N^{\rm A}$—3 with $N^{\rm A}$ equal to the number of atoms), $\sigma_{\rm sym}$ is an identical-atom permutational symmetry number, which for CH_4 is 4!, and $\rho(\mathbf{x},T)$ is the quantum mechanical coordinate-space density at temperature T.

We use isoinertial coordinates, in particular, rectilinear coordinates scaled to a reduced mass μ, in which case the QM density may be calculated by the Feynman path integral method as

$$\rho = \oint D[\mathbf{x}(s)] \exp\left\{-\frac{1}{\hbar}\int_0^{\beta\hbar} ds \left(\frac{\mu}{2}\left(\frac{d\mathbf{x}}{ds}\right)^2 + V[\mathbf{x}(s)]\right)\right\}, \tag{2}$$

where $\beta = 1/k_B T$, k_B is Boltzmann's constant, V is the potential energy, $\hbar$ is Planck's constant divided by 2π, and $\oint D[\mathbf{x}(s)]\ldots$ denotes a path integral, that is, the summation over all closed paths beginning and ending at $\mathbf{x}$ and parameterized by the modulus s of the imaginary time over which the path is traversed. The partition function may then be re-expressed as

$$Q = \frac{1}{\sigma_{\rm sym}} \int_{-\infty}^{\infty} d\mathbf{x} \oint D[\mathbf{x}(s)] \Phi^{\rm fp}[\mathbf{x}(s)] \times \exp\left\{-\frac{1}{\hbar}\int_0^{\hbar\beta} ds V[\mathbf{x}(s)]\right\}, \tag{3}$$

where $\Phi^{\rm fp}[\mathbf{x}(s)]$ denotes the contribution of a particular path to a free particle density, $\rho^{\rm fp}$, i.e.,

$$\rho^{\rm fp} = \oint D[\mathbf{x}(s)]\, \Phi^{\rm fp}[\mathbf{x}(s)] = \oint D[\mathbf{x}(s)] \exp\left[-\frac{1}{\hbar}\int_0^{\hbar\beta} ds \frac{\mu}{2}\left(\frac{d\mathbf{x}}{ds}\right)^2\right]. \tag{4}$$

In order to allow convenient Monte Carlo sampling, we multiply and divide the right hand side of Eq. (3) by the partition function of a free particle, and we restrict the configuration space to a finite domain Γ (which will be taken large enough to achieve converged results). This yields

$$Q = \frac{Q_{\rm fp}(T)}{\sigma_{\rm sym}} \times \frac{\int_\Gamma d\mathbf{x} \oint D[\mathbf{x}(s)]\ \Phi^{\rm fp}[\mathbf{x}(s)] \exp\left\{-\frac{1}{\hbar}\int_0^{\hbar\beta} ds\, V[\mathbf{x}(s)]\right\}}{\int_\Gamma d\mathbf{x} \oint D[\mathbf{x}(s)]\ \Phi^{\rm fp}[\mathbf{x}(s)]}, \tag{5}$$

where $Q_{\rm fp}$ is the contribution to a free-particle partition function that comes from paths that begin and end at a point within Γ; this quantity is given by

$$Q_{\rm fp} = V_\Gamma \left(\frac{\mu}{2\pi\beta\hbar^2}\right)^{N/2}, \tag{6}$$

where V_Γ is the volume of the restricted domain. If the integration over s is done by trapezoidal-rule quadrature, then Eq. (5) becomes

$$Q^{[P]} = \frac{Q_{\rm fp}(T)}{\sigma_{\rm sym}} \times \frac{\int_\Gamma d\mathbf{x}_1 \oint D[\mathbf{x}(s)]\ \Phi^{\rm fp}[\mathbf{x}(s)]\ \exp\left\{-\frac{\beta}{P}\sum_{i=1}^{P} V(\mathbf{x}_i)\right\}}{\int_\Gamma d\mathbf{x}_1 \oint D[\mathbf{x}(s)]\ \Phi^{\rm fp}[\mathbf{x}(s)]}. \tag{7}$$

The outer quadratures in Eq. (7) involve the initial path position, but when developing importance sampling schemes (as we shall discuss below), the paths are better characterized by their centroid position $\mathbf{x}_{\rm C}$, which for the path $\mathbf{x}_1, \mathbf{x}_2, \ldots, \mathbf{x}_P$ is given by

$$\mathbf{x}_{\rm C} = \frac{1}{P}\sum_{i=1}^{P} \mathbf{x}_i. \tag{8}$$

Note that this definition of the centroid depends on P, so $\mathbf{x}_{\rm c}$ is different for different P's. The centroid analog of Eq. (7) is then given by

$$Q^{[P]} = \frac{Q_{\rm fp}(T)}{\sigma_{\rm sym}} \frac{\int_\Gamma d\mathbf{x}_{\rm c} \oint D[\mathbf{x}(s)]\ \Phi^{\rm fp}[\mathbf{x}(s)] \exp\left\{-\frac{\beta}{P}\sum_{i=1}^{P} V(\mathbf{x}_i)\right\} \delta\left\{\mathbf{x}_{\rm c} - \frac{1}{P}\sum_{i=1}^{P}\mathbf{x}_i\right\}}{\int_\Gamma d\mathbf{x}_{\rm c} \oint D[\mathbf{x}(s)]\ \Phi^{\rm fp}[\mathbf{x}(s)] \delta\left\{\mathbf{x}_{\rm c} - \frac{1}{P}\sum_{i=1}^{P}\mathbf{x}_i\right\}}. \tag{9}$$

We carry out Monte Carlo integration using uncorrelated sampling of centroid configurations, which allows for straightforward uncertainty estimates (whereas the more popular Metropolis algorithm does not allow so). After selecting a centroid configuration, we calculate a path, starting at some arbitrary initial configuration, according to a free-particle distribution (i.e., the distribution for the case where $V = 0$) and then re-center this path at $\mathbf{x}_c$. (There are a variety of algorithms for generating Feynman paths according to a free particle distribution; we use the sequential sectioning scheme discussed in detail previously.[48]) The Monte Carlo integration of Eq. (9) with uniform sampling of $\mathbf{x}_c$ may conveniently be expressed as

$$Q^{[P]} = \frac{Q_{\rm fp}(T)}{\sigma_{\rm sym}} \left\langle \exp\left\{ -\frac{\beta}{P} \sum_{i=1}^{P} V(\mathbf{x}_i) \right\} \right\rangle_{\rm fp,\, \mathbf{x}_c}, \qquad (10)$$

where $\langle \ldots \rangle_{\rm fp,\, \mathbf{x}_c}$ denotes an average of the bracketed quantity with paths sampled according to a free-particle distribution and with centroid positions chosen uniformly from within Γ.

B. Importance sampling

Uniformly sampling within Γ is too inefficient for practical work, so we modify Eq. (10) by importance sampling using an unnormalized importance function denoted f. Equation (10) then becomes

$$Q^{[P]} = \frac{Q_{\rm fp}(T)\langle f \rangle}{\sigma_{\rm sym}} \left\langle \frac{1}{f(\mathbf{x}_c)} \exp\left\{ -\frac{\beta}{P} \sum_{i=1}^{P} V(\mathbf{x}_i) \right\} \right\rangle_{{\rm fp},f(\mathbf{x}_c)}, \qquad (11)$$

where $\langle f \rangle$ denotes the average value of f over the integration domain.

For the calculations presented here, we employ mass-scaled generalized[51] Jacobi (GJ) coordinates (hereafter simply referred to as GJ coordinates) given by

$$\mathbf{x}_c = \sqrt{\frac{\mu_1}{\mu}}\mathbf{y}_1 \otimes \sqrt{\frac{\mu_2}{\mu}}\mathbf{y}_2 \otimes \sqrt{\frac{\mu_3}{\mu}}\mathbf{y}_3 \otimes \sqrt{\frac{\mu_4}{\mu}}\mathbf{y}_4, \qquad (12)$$

where $\mathbf{y}_1$ is an unscaled three-vector pointing from $H_{(1)}$ to C, $\mathbf{y}_2$ is a three-vector pointing from $H_{(2)}$ to the center of mass of $CH_{(1)}$, $\mathbf{y}_3$ is a three-vector pointing from $H_{(3)}$ to the center of mass of $CH_{(1)}H_{(2)}$, and $\mathbf{y}_4$ is a three-vector pointing from $H_{(4)}$ to the center of mass of $CH_{(1)}H_{(2)}H_{(3)}$. The μ_i are reduced masses given by $m_i\tilde{m}_i/(m_i + \tilde{m}_i)$, where m_i and $\tilde{m}_i$ are the masses of the two fragments connected by the vector $\mathbf{y}_i$, and μ is a scaling mass taken here to be the mass of an electron. The sampling domain is defined by specifying upper and lower bounds on the magnitudes of each of the $\mathbf{y}_i$.

Our importance function will be taken as a product of nine 1-dimensional functions; four will be associated with the magnitudes of the GJ three-vectors, $y_i^{\rm M} = |\mathbf{y}_i|$, three will be associated with the angles, θ_i, between consecutive GJ vector pairs $\mathbf{y}_i$ and $\mathbf{y}_{i+1}$, and two will be associated with the dihedral angles, τ_i, between consecutive GJ vector triples $\mathbf{y}_i$, $\mathbf{y}_{i+1}$, and $\mathbf{y}_{i+2}$ (the angle between the plane containing $\mathbf{y}_i$ and $\mathbf{y}_{i+1}$ and the plane containing $\mathbf{y}_{i+1}$ and $\mathbf{y}_{i+2}$). As in previous work,[45] we will use Gaussian functions for the distribution of the GJ vector magnitudes and GJ vector angle degrees of freedom where the center parameters will be taken from the equilibrium configuration and the width parameters will be optimized. Our dihedral importance sampling functions will be defined between −180° and 180° and will contain two domains of high probability, where the probability of acceptance is unity, with the remaining space having a lower acceptance probability that is determined so that the probability of being within the two high-probability domains occurs with a specified probability $p_i^{\rm tor}$ (which is an input parameter), i.e.,

$$f_i^{\rm tor}(\tau_i) = \begin{cases} 1; & \text{if } \left|\tau_i - \tau_{o,i}^{(1)}\right| < \Delta_{\tau_i}^{(1)}/2 \\ 1; & \text{if } \left|\tau_i - \tau_{o,i}^{(2)}\right| < \Delta_{\tau_i}^{(2)}/2 \\ \varepsilon_i; & \text{otherwise} \end{cases}, \qquad (13)$$

where we express ε_i in terms of the probability $p_i^{\rm tor}$ via

$$\varepsilon_i = \frac{\left(\Delta_{\tau_i}^{(1)} + \Delta_{\tau_i}^{(2)}\right)\left(1 - p_i^{\rm tor}\right)}{p_i^{\rm tor}\left(2\pi - \left[\Delta_{\tau_i}^{(1)} + \Delta_{\tau_i}^{(2)}\right]\right)}. \qquad (14)$$

The combined importance function used for the calculations in this article has the form

$$f(\mathbf{x}) = f_1^{\rm tor}(\tau_1) f_2^{\rm tor}(\tau_2) \prod_{j=1}^{3} \exp\left(-\frac{\left(\theta_j - \theta_{0,j}\right)^2}{2\Delta_{\theta_j}^2} \right) \times \prod_{i=1}^{4} \exp\left(-\frac{\left(y_i^{\rm M} - y_{i,0}^{\rm M}\right)^2}{2\Delta_i^2} \right). \qquad (15)$$

By using two random deviates, one to determine whether the sample falls inside or outside the high-probability segments and the second to determine the location within the indicated subdomain, it is straightforward to sample a dihedral degree of freedom according to the function of Eq. (13) without using rejection methods. We sample the GJ vector magnitudes and GJ vector angles using a ziggurat scheme,[45,52] discussed in detail previously,[45] that allows samples to be drawn from a distribution consisting of a Gaussian times the appropriate Jacobian (either the square of a magnitude or the sine of an angle). This approach involves almost no rejection; thus, the cost of generating a configuration distributed according to the importance function of Eq. (15) is only slightly higher than the cost of 18 uniform random numbers.

C. Stratification

In addition to importance sampling, we also employ adaptively optimized[41] stratification in our calculations. We first partition Γ into several disjoint strata k of volume V_k and generalize Eq. (11) to

$$Q^{[P]} = \frac{1}{\sigma_{\rm sym}} \sum_{k=1}^{N^{\rm strata}} Q_k^{\rm fp}(T)\langle f \rangle_k \times \left\langle \frac{1}{f(\mathbf{x}_c)} \exp\left\{ -\frac{\beta}{P} \sum_{i=1}^{P} V(\mathbf{x}_i) \right\} \right\rangle_{{\rm fp},f(\mathbf{x}_c);k}, \qquad (16)$$

where $\langle \ldots \rangle_{{\rm fp},f(\mathbf{x}_c);k}$ denotes an average of the bracketed quantity over all $\mathbf{x}_c$ values (sampled via the importance function f) within stratum k and averaged over all free particle paths

centered at these $\mathbf{x}_c$, Q_k^{fp} denotes the contribution of stratum k to the free-particle partition function, and

$$\langle f\rangle_k = \frac{1}{V_k}\int_{\Gamma_k} d\mathbf{x}_c f(\mathbf{x}_c). \quad (17)$$

As discussed further below, our strata will be defined such that the V_k, which are needed to calculate the Q_k^{fp}, as well as the $\langle f\rangle_k$, are not readily available. We therefore choose to rewrite Eq. (16) in the form

$$Q^{[P]} = \frac{Q^{fp}(T)\langle f\rangle}{\sigma_{sym}} \times \sum_{k=1}^{N^{strata}} \alpha_k \left\langle \frac{1}{f(\mathbf{x}_c)} \exp\left\{-\frac{\beta}{P}\sum_{i=1}^{P} V(\mathbf{x}_i)\right\}\right\rangle_{fp,f(\mathbf{x}_c);k}, \quad (18)$$

where

$$\alpha_k = \frac{\langle f\rangle_k V_k}{\langle f\rangle V}. \quad (19)$$

The α_k are then calculated as the fraction of candidate centroid samples obtained with importance function f that falls within stratum k. We estimate the α_k on the fly and they typically converge much faster than the partition function does; thus, the uncertainties in the α_k values are negligible compared to the uncertainties in the rest of the calculation.

We distribute an initial fraction of the total number of samples (typically 5%–10%) in one of two ways: we either distribute them in a "strata-blind" fashion, so that the strata are initially populated based only on the importance function, or we distribute samples so that each stratum is assigned the same number of samples. We chose the second option for the calculations in the present work; this helps ensure that no stratum is under-sampled during the initial sampling phase (if a stratum is under-sampled in the initial sampling phase and spuriously estimated to have a small contribution to the total partition function, it might never be sampled again in subsequent phases, which would result in incorrect results). After the initial sampling phase, the remaining samples are distributed in a number of stages (typically 5–20), which we sometimes refer to as "sweeps." Before each of these sweeps, we calculate[41] an optimal distribution for further samples based on the most current estimate of the strata variances.

Previously[48] we defined our strata as evenly spaced intervals of the centroid energy; energy stratification is very robust, but because this requires distributing samples among the strata by rejection sampling, it involves a very significant overhead (in some cases, hundreds of candidate samples must be considered for each accepted configuration). We now generalize our approach to include some strata based only on geometric information because this is typically much less expensive to calculate than the energy. In particular, we define our geometry-based strata with the goal that when most of the high-energy configurations that are oversampled by our importance function are rejected, it is done without the expense of an energy evaluation. This is accomplished as follows. First, we define some geometric criteria, and a portion of the sampling domain is divided into strata based on these geometrical criteria. Then the residual sampling domain, which typically includes all of the most important configuration space, is divided based on the centroid configuration energy as before[48] except for one modification: the energy range of the lowest-energy stratum is allowed to be different from (and typically chosen to be larger than) that of the remaining energy-based strata (all the energy-based strata except for the first and last are defined based on a common energy spacing parameter; the last stratum includes all energies not included in the other strata). We do this because if the first energy-based stratum is given an energy range that is the same as for the other energy-based strata, its configuration space volume would be very small compared with that of the other strata, and thus, the requirement that each stratum receive the same number of samples in the initial sampling phase would result in requiring an unnecessarily large number of samples for this stratum (which can result in very high sampling costs because we need to select samples from the entire sample domain and rejection sample based on the centroid energy until we find the needed number of samples for each stratum).

D. Harmonically guided variance reduction (HGVR)

In cases where a Hessian evaluation of either the true potential or a reference potential is affordable, we can use the HGVR scheme,[49] which makes the replacement in Eq. (18),

$$\exp\left\{-\frac{\beta}{P}\sum_{i=1}^{P} V(\mathbf{x}_i)\right\} \to \exp\left\{-\frac{\beta}{P}\sum_{i=1}^{P} V(\mathbf{x}_i)\right\} + \Delta^{HGVR}(\mathbf{x}_c), \quad (20)$$

where

$$\Delta^{HGVR}(\mathbf{x}_c) = \left\langle \exp\left\{-\frac{\beta}{P}\sum_{i=1}^{P} V^{ref,HO}(\mathbf{x}_i)\right\}\right\rangle_{fp} - \exp\left\{-\frac{\beta}{P}\sum_{i=1}^{P} V^{ref,HO}(\mathbf{x}_i)\right\} \quad (21)$$

and $V^{ref,HO}(\mathbf{x}_i)$ denotes a harmonic approximation of the reference potential [restricted to include only those instantaneous normal modes[53] (INMs) with positive frequencies]. In the calculations presented in this article, we use the true potential to calculate the INM frequencies needed to form $V^{ref,HO}(\mathbf{x}_i)$.

The first term on the right hand side of Eq. (21) involves an average over all paths and has an analytical solution

$$\left\langle \exp\left\{-\frac{\beta}{P}\sum_{i=1}^{P} V^{ref,HO}(\mathbf{x}_i)\right\}\right\rangle_{fp} = \frac{W_S^{[1]}}{W_S^{[P]}} \exp\left(-\beta V^{ref,HO}(\mathbf{x}_c)\right), \quad (22)$$

where

$$W_S^{[P]} = \prod_{m,\omega_m^2>0} \frac{q_m^{HO}(\omega_m)}{q_m^{HO,P}(\omega_m)}. \quad (23)$$

The ω_m are the INM frequencies evaluated at $\mathbf{x}_c$, $q_m^{HO}(\omega_m)$ is the exact harmonic oscillator (HO) partition function, and $q_m^{HO,P}(\omega_m)$ is the finite-P approximation of the HO partition function given by[54]

$$q_m^{HO,P} = \frac{f(\omega_m)^{P/2}}{f(\omega_m)^P - 1}, \tag{24}$$

where

$$f(\omega_m) = 1 + \frac{R_m^2}{2} + \frac{R_m}{2}\sqrt{4 + R_m^2} \tag{25}$$

and

$$R_m = \frac{\hbar\beta\omega_m}{P}. \tag{26}$$

Δ^{HGVR} is zero after averaging over an infinite number of paths. The advantage of Eq. (21) arises when it is averaged over only one or a few paths; in which case $-\Delta^{HGVR}$ is an approximation of the statistical error when averaging $\exp\left\{-\frac{\beta}{P}\sum_{i=1}^{P} V(\mathbf{x}_i)\right\}$ over this limited set of paths. Thus, use of Eq. (20) leads to lower statistical uncertainties during Monte Carlo sampling; at intermediate temperatures, this can lead to convergence being accelerated by more than an order of magnitude.[49]

E. Extrapolation

Our early path integral work[40,41,55,56] represented the Feynman paths using a Fourier expansion having K degrees of freedom per dimension; this approach displays only $O(K^{-1})$ convergence but can be readily extrapolated[40] by fitting results from calculations with several different values of K to the expression

$$Q^{[K]} = Q^{[K=\infty]} + \frac{C_1}{K} + \frac{C_2}{K^2} \tag{27}$$

to achieve at least $O(K^{-2})$ convergence, where the C_i and $Q^{[K=\infty]}$ are fitting parameters. Eventually, we adopted an isomorphism of Coalson[57] that allowed a $P = K + 1$ term rescaled Fourier expansion to generate a P-point discretized representation, which we extrapolated by fitting results for several different values of K to

$$Q^{[K]} = Q^{[K=\infty]} + \frac{C_2}{K^2} + \frac{C_3}{K^3} \tag{28}$$

which results in $O(K^{-4})$ convergence. We subsequently found it convenient to express all our notation in terms of P instead of K and have replaced Fourier-like representations of free-particle paths with a sequential sectioning scheme.[48] We thus rewrote Eq. (28) as

$$Q^{[P]} = Q^{[P=\infty]} + \frac{C_2}{P^2} + \frac{C_3}{P^3}. \tag{29}$$

(Extrapolations including terms up to order P^{-2} had also been considered by other groups.[58–60]) However, we now realize that whereas odd powers of K are needed in Eq. (28), only even powers of P are needed[59,61] in Eq. (29) so we are switching to use of the expression

$$Q^{[P]} = Q^{[P=\infty]} + \sum_{j=1}^{n-1} \frac{C_{2j}}{P^{2j}} + O\left[P^{-2n}\right]. \tag{30}$$

We will restrict attention to fits using the same number of data points as parameters.

Extrapolating data that are subject to statistical uncertainty can potentially magnify errors; a key feature of our extrapolation process is that our partition function estimates for different values of P are all highly correlated. In particular, we obtain our estimates from different integrations of the same set of paths. During the calculations, our paths are only uniquely specified at a set of P_{max} points, so we are restricted to obtaining estimates, $Q^{[P]}$, where P is a divisor of P_{max}. We use the enhanced same path (ESP) extrapolation scheme[44] whereby we average P_{max}/P different quadrature estimates of the contribution of each path to $Q^{[P]}$, and this leads to monotonic convergence on a path-by-path basis.

There are two subtle complications with ESP calculations when $P \neq P_{max}$, both related to the fact that the centroid of a subset of P points differs slightly from the centroid of the full set of P_{max} points, as pointed out after Eq. (8); thus when $P < P_{max}$, our calculations will only approximate $Q^{[P]}$ values, although the deviations are typically very slight and do not appreciably affect the extrapolated results that are our primary goal. The first complication relates to the fact that we use importance sampling based on the centroid configuration, and the second relates to the fact that Eq. (22) of the HGVR correction scheme is only strictly valid if the INM frequencies are calculated at the P-point centroid configuration, whereas we use the P_{max} centroid for all P.

The first complication can lead to a result that differs slightly from $Q^{[P]}$. This has been extensively tested numerically by using a code option to re-center each path to perfectly match the centroid. Such paths are very similar as a function of P, so they extrapolate reasonably well, but using this option requires making new energy calculations for each path because now the quadrature nodes for paths with different P's do not perfectly coincide. In the absence of stratification, we would get the exact value of $Q^{[P]}$ if the *contribution* of the path centered at the P_{max} centroid is the same as the contribution of the path re-centered at the P-point centroid, but we would also get the exact result if the *weight* of the P_{max} centroid is the same as the weight of the P-point centroid even if the path contributions are different. We get equal weights with uniform sampling, and we get both equal contributions and equal weights as $P \to \infty$. In practice, we find that except for low T and low P, deviations from a rigorously calculated value of $Q^{[P]}$ due to this effect are negligible. If one is interested in converging several $Q^{[P]}$ values to very high accuracy for their own sake, one should re-center the paths; but here our goal is only to obtain an accurate extrapolated result, and because the employed approximations of $Q^{[P]}$ extrapolate to the same limit as the accurate values, we use the less expensive option.

The second complication, relating to the HGVR treatment, can be more significant, but it is typically only appreciable for P values at which $Q^{[P]}$ is a qualitatively incorrect estimate of the converged partition function. Both effects decrease to zero in the $P \to \infty$ limit but may not do so with the same asymptotic behavior as predicted by Eq. (30). We tabulate two or more different extrapolation estimates and any errors introduced by these subtle effects would be reflected in the differences between these estimates; however, when comparing our $Q^{[P]}$

values (for $P < P_{\max}$) to highly accurate estimates of $Q^{[P]}$ from other methods, it would be helpful to remember that these effects are not reflected in our uncertainty estimates. As a practical matter, the primary consequence of these two effects is that we cannot use the ESP scheme to calculate the classical (i.e., $P = 1$) partition function, so we instead use the energy from the centroid configuration to obtain the classical result.

It is convenient to express the results of fits to Eq. (30) for several values of P in the form

$$Q^{[P=\infty]} = Q^{[P_{\max}]} + \sum_{i=1}^{n-1} \alpha_i \left(Q^{[P_{\max}/d_i]} - Q^{[P_{\max}]} \right) + O\left[P_{\max}^{-2n}\right], \tag{31}$$

where the coefficients α_i depend on the values of the divisors d_i but are *independent* of $P_{\max}$. Thus, for example, this extrapolation treatment could be extended to cases where different values of P are used for different dimensions, as considered by Steele *et al.*,[62] provided that the same set of divisors is used (we only consider the case where the same discretization is used for all dimensions because the realistic potentials we have considered cannot readily be written into a form that would permit us to take advantage of different discretizations). Another advantage of casting the extrapolation in the form of Eq. (31) is that we can affordably perform the extrapolation on a path-by-path basis, which allows us to directly obtain statistical uncertainty estimates for the $P = \infty$ estimations. We typically observe that, except for very small values of P, the relative uncertainties, i.e., the absolute uncertainties divided by the partition function, of the $Q^{[P]}$ data are nearly independent of P; thus, because the partition function monotonically decreases with P, the absolute uncertainty estimates we obtain for the extrapolated partition functions can be smaller than those for the $Q^{[P_{\max}]}$ calculations provided that we choose $P_{\max}$ sufficiently large to yield reasonably converged values. For small values of $P_{\max}$, the extrapolated data can exhibit substantially larger relative statistical uncertainties than the data for $P_{\max}$; this issue will be explored further in Sec. IV.

It is straightforward to re-express extrapolations based on Eq. (30) in the form of Eq. (31). We start by selecting n values of $P(P_{\max}, P_{\max}/d_1, \ldots, P_{\max}/d_{n-1})$ and substitute these into Eq. (30) giving us a set of n equations in n unknowns,

$$\begin{bmatrix} 1 & \frac{1}{P_{\max}^2} & \cdots & \frac{1}{P_{\max}^{2(n-1)}} \\ 1 & \frac{d_1^2}{P_{\max}^2} & \cdots & \frac{d_1^{2(n-1)}}{P_{\max}^{2(n-1)}} \\ \vdots & \vdots & \ddots & \vdots \\ 1 & \frac{d_{n-1}^2}{P_{\max}^2} & \cdots & \frac{d_{n-1}^{2(n-1)}}{P_{\max}^{2(n-1)}} \end{bmatrix} \begin{bmatrix} Q^{[P=\infty]} \\ C_2 \\ \vdots \\ C_{2(n-1)} \end{bmatrix} = \begin{bmatrix} Q^{[P_{\max}]} \\ Q^{[P_{\max}/d_1]} \\ \vdots \\ Q^{[P_{\max}/d_{n-1}]} \end{bmatrix}. \tag{32}$$

Solving Eq. (32) for $Q^{[P=\infty]}$ gives us an answer that is a linear combination of $Q^{[P_{\max}]}$ and the $Q^{[P_{\max}/d_i]}$, and it is easy to see that if we re-express this as a linear combination of $Q^{[P_{\max}]}$ and the $\left(Q^{[P_{\max}/d_i]} - Q^{[P_{\max}]}\right)$, then the coefficient for the $Q^{[P_{\max}]}$ term is unity. The most useful 2-point extrapolation formula, restricted to cases where $2|P_{\max}$ (where this notation indicates that 2 is a divisor of $P_{\max}$) is

$$Q^{[P=\infty]} = Q^{[P_{\max}]} - \frac{1}{3}\left(Q^{[P_{\max}/2]} - Q^{[P_{\max}]}\right) + O\left[P_{\max}^{-4}\right]. \tag{33}$$

We will consider 3-point formulas for cases where $6|P_{\max}$

$$Q^{[P=\infty]} = Q^{[P_{\max}]} - \frac{3}{5}\left(Q^{[P_{\max}/2]} - Q^{[P_{\max}]}\right) + \frac{1}{10}\left(Q^{[P_{\max}/3]} - Q^{[P_{\max}]}\right) + O\left[P_{\max}^{-6}\right] \tag{34}$$

and where $4|P_{\max}$

$$Q^{[P=\infty]} = Q^{[P_{\max}]} - \frac{4}{9}\left(Q^{[P_{\max}/2]} - Q^{[P_{\max}]}\right) + \frac{1}{45}\left(Q^{[P_{\max}/4]} - Q^{[P_{\max}]}\right) + O\left[P_{\max}^{-6}\right]. \tag{35}$$

For 4-point formulas, we consider cases where $12|P_{\max}$

$$Q^{[P=\infty]} = Q^{[P_{\max}]} - \frac{4}{5}\left(Q^{[P_{\max}/2]} - Q^{[P_{\max}]}\right) + \frac{8}{35}\left(Q^{[P_{\max}/3]} - Q^{[P_{\max}]}\right) - \frac{1}{35}\left(Q^{[P_{\max}/4]} - Q^{[P_{\max}]}\right) + O\left[P_{\max}^{-8}\right], \tag{36}$$

where $6|P_{\max}$

$$Q^{[P=\infty]} = Q^{[P_{\max}]} - \frac{27}{40}\left(Q^{[P_{\max}/2]} - Q^{[P_{\max}]}\right) + \frac{2}{15}\left(Q^{[P_{\max}/3]} - Q^{[P_{\max}]}\right) - \frac{1}{840}\left(Q^{[P_{\max}/6]} - Q^{[P_{\max}]}\right) + O\left[P_{\max}^{-8}\right], \tag{37}$$

and where $8|P_{\max}$

$$Q^{[P=\infty]} = Q^{[P_{\max}]} - \frac{64}{135}\left(Q^{[P_{\max}/2]} - Q^{[P_{\max}]}\right) + \frac{4}{135}\left(Q^{[P_{\max}/4]} - Q^{[P_{\max}]}\right) - \frac{1}{2835}\left(Q^{[P_{\max}/8]} - Q^{[P_{\max}]}\right) + O\left[P_{\max}^{-8}\right]. \tag{38}$$

For 5-point formulas, we consider this case where $12|P_{\max}$

$$Q^{[P=\infty]} = Q^{[P_{\max}]} - \frac{9}{10}\left(Q^{[P_{\max}/2]} - Q^{[P_{\max}]}\right) + \frac{32}{105}\left(Q^{[P_{\max}/3]} - Q^{[P_{\max}]}\right) - \frac{9}{175}\left(Q^{[P_{\max}/4]} - Q^{[P_{\max}]}\right) + \frac{1}{1050}\left(Q^{[P_{\max}/6]} - Q^{[P_{\max}]}\right) + O\left[P_{\max}^{-10}\right]. \tag{39}$$

In all these cases, we see that the α_i coefficients alternate in sign and decrease monotonically and rapidly as i increases; in particular, the coefficients are well behaved in the sense that they decrease more rapidly than d_i^{-2}; thus, at least asymptotically, terms involving lower-P values of $Q^{[P]}$ contribute less than higher-P terms.

In order to further explore the behavior of the extrapolation formulas considered above, we test their performance for a one-dimensional harmonic oscillator; this is facilitated by the analytical formulas[54] for the finite-P partition functions of Eqs. (24)–(26) that allow us to determine the extrapolation formula errors exactly for this case. First, we consider the relative effectiveness of different formulas of the same order. Our numerical tests show that, asymptotically, the three-point formula of Eq. (34) has an error that is a factor of 1.78 times more accurate than the 3-point formula of Eq. (35). This can be understood by the observation that the 4-point formula of Eq. (36), which is accurate to $O(P^{-8})$, cancels the $O(P^{-6})$ error by taking a linear combination of 16/7 times Eq. (34) and −9/7 times Eq. (35); thus, Eq. (34) must be asymptotically 16/9 times as accurate as Eq. (35) for *any* interaction potential and any T. Of the 4-point formulas, asymptotically, Eq. (36) is a factor of 9/4 more accurate than Eq. (37) and a factor of 64/9 more accurate than Eq. (38). These results suggest that the most accurate formula for any given order is the one with the smallest divisors, d_i. Unfortunately, the most accurate formulas for any given order are also the ones for which the set of d_i have the largest least common multiples (LCMs). The LCM must be a divisor of $P_{\max}$, so selecting formulas with large LCMs limits us to the use of larger values of $P_{\max}$ than would otherwise be the case, and this complication is exacerbated as we increase the order of the extrapolation (for example, the 7-point formula that is optimal from an accuracy standpoint would have a LCM of 420). In selecting for further study of the 5-point formula of Eq. (39), we disregard the formula resulting from choosing divisors of 2, 3, 4, and 5 because this result, which would be marginally more accurate (by a factor of 36/25 asymptotically) than Eq. (39), requires that $P_{\max}$ be a multiple of 60, which would restrict its applicability to low temperatures, and if we were to be interested in such cases, this 6-point formula

$$\begin{aligned} Q^{[P=\infty]} = {} & Q^{[P_{\max}]} - \frac{15}{14}\left(Q^{[P_{\max}/2]} - Q^{[P_{\max}]}\right) \\ & + \frac{10}{21}\left(Q^{[P_{\max}/3]} - Q^{[P_{\max}]}\right) \\ & - \frac{1}{7}\left(Q^{[P_{\max}/4]} - Q^{[P_{\max}]}\right) \\ & + \frac{2}{77}\left(Q^{[P_{\max}/5]} - Q^{[P_{\max}]}\right) \\ & - \frac{1}{462}\left(Q^{[P_{\max}/6]} - Q^{[P_{\max}]}\right) + O\left[P_{\max}^{-12}\right] \end{aligned} \quad (40)$$

might be more appropriate.

Next, we consider the performance of various extrapolation orders; Figure 1 displays results for a harmonic oscillator with $\omega = 3000\ \mathrm{cm}^{-1}$ at temperatures of 100 K and 500 K and compares the primitive $Q^{[P]}$ results to results of extrapolation schemes using 2–5 data points. One thing to note from the 100 K data is that, in the low-P regime, higher-order schemes do not always guarantee higher accuracy, although this is true at this T by the point that useful accuracy is achieved. It is also important to realize that the C_{2j} coefficients in Eq. (30) contain a strong β dependence; thus, changing from an n-point extrapolation formula to an $(n+1)$-point extrapolation

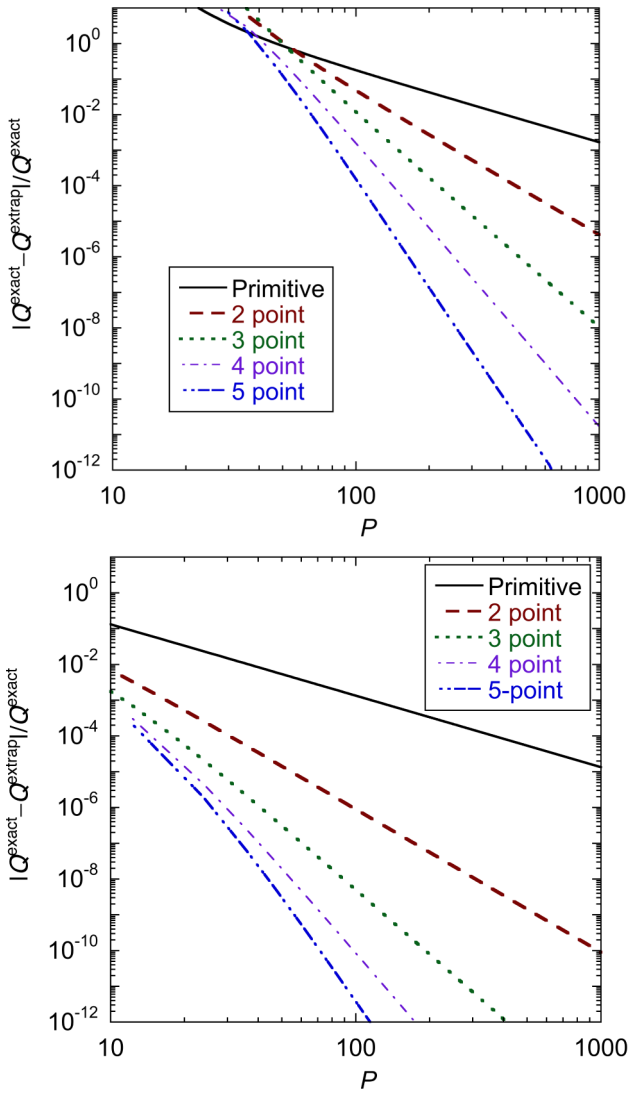

FIG. 1. A comparison of relative errors vs. P for primitive $Q^{[P]}$ calculations and various extrapolation schemes [Eqs. (33), (34), (36), and (39)] for the case of a one-dimensional harmonic oscillator with $\omega = 3000\ \mathrm{cm}^{-1}$. (a) $T = 100$ K, (b) $T = 500$ K.

formula does not yield anything like a factor of $P_{\max}^2$ increase in accuracy that one might naively have expected.

Often it is convenient to have an explicit test of the accuracy of the extrapolated results. One way to do this is by comparing results of different orders, but we can also check convergence by omitting the $P_{\max}$ data point and relying on only the lower-P data using formulas such as these (both appropriate for $12|P_{\max}$)

$$\begin{aligned} Q^{[P=\infty]} = {} & Q^{[P_{\max}/2]} - \frac{128}{70}\left(Q^{[P_{\max}/3]} - Q^{[P_{\max}/2]}\right) \\ & + \frac{3}{7}\left(Q^{[P_{\max}/4]} - Q^{[P_{\max}/2]}\right) + O\left[P_{\max}^{-6}\right], \end{aligned} \quad (41)$$

$$\begin{aligned} Q^{[P=\infty]} = {} & Q^{[P_{\max}/2]} - \frac{256}{105}\left(Q^{[P_{\max}/3]} - Q^{[P_{\max}/2]}\right) \\ & + \frac{27}{35}\left(Q^{[P_{\max}/4]} - Q^{[P_{\max}/2]}\right) \\ & - \frac{1}{30}\left(Q^{[P_{\max}/6]} - Q^{[P_{\max}/2]}\right) + O\left[P_{\max}^{-8}\right]. \end{aligned} \quad (42)$$

We note that these equations have a tighter spacing of P values than that which is possible for formulas that use the $P_{\max}$ data point and this results in increased accuracy; thus, for example, Eq. (41) is asymptotically only a factor of 16 less accurate than Eq. (33) for a given value of $P_{\max}$ whereas we might have expected a factor of $2^6 = 64$ decrease in accuracy based only on the convergence order.

In addition to extrapolation, there are a variety of other methods that achieve either cubic[63–69] or quartic[70–73] convergence with respect to the number of discretized points or similar path representation parameters (for example, Fourier expansion coefficients), with the quartic scheme of Predescu,[70] which, in contrast to many of the other methods, does not require higher-order derivatives, being among the most noteworthy. Cumulant expansion methods[74] and other schemes[75,76] have also been proposed as a means of achieving convergence rates that are even faster than quartic. In light of the very high convergence rates demonstrated here, the negligible cost beyond that of the primitive discretized scheme, and the simplicity of the method, we conclude that the ESP extrapolation procedure compares very favorably with these competing methods.

III. CALCULATIONS

All our previous path integral work, as well as the formulation outlined in Sec. II, have been for vibrational–rotational partition functions without consideration of nuclear spin effects. However, Chakraborty *et al.*[2] have included a factor of $(2I+1)^4 = 16$ (where $I = 1/2$ is the nuclear spin of a hydrogen atom) to account for the effects of nuclear spin states in the limit that these can be treated by an average weight of all states (which, for methane or heavier molecules, is valid even for temperatures well below the lowest T value considered here). We will thus include a factor of 16 in our results as well in order to facilitate direct comparisons to the earlier results. We note, as an aside, that Wilson[77] has discussed in detail the statistical weights associated with individual rovibrational levels, and this treatment may be used to calculate accurate partition functions with Boltzmann factor summation at low T. Procedures to treat such effects rigorously in path integral calculations have also been discussed.[20]

We have performed partition function calculations for 13 temperatures in the 300–3000 K temperature range. The masses used in the calculations are 12 and 1.007 825 032 07 amu for C and H, respectively. The numerical parameters for the calculations are given in Table I, the results for various values of P and for several different extrapolation schemes are given in Table II, and a comparison of the path integral results to classical partition functions (from $P = 1$ calculations) and VCI calculations is given in Table III.

In addition to the partition functions, we also tabulate enthalpies, entropies, and heat capacities. To be consistent with standard practice in thermochemical tables, we include translational contributions[1] for an ideal gas at a pressure of 1 bar but *do not* include the factor of 16 for the nuclear spin contribution to the partition function when calculating these quantities. The following expressions are used to calculate the vibrational–rotational contribution to the thermodynamic functions:

$$A = -k_B T \ln Q, \tag{43}$$

$$\langle E \rangle = -\frac{\partial \ln Q}{\partial \beta}, \tag{44}$$

$$S = k_B(\ln Q + \beta \langle E \rangle), \tag{45}$$

$$C_V = k_B \beta^2 \frac{\partial^2 \ln Q}{\partial \beta^2}. \tag{46}$$

We perform these calculations with the extrapolated values of Q [using the 4-point scheme of Eq. (36)], and the partial derivatives in Eqs. (44) and (46) are evaluated by finite differences using three highly correlated values of Q obtained by simultaneously performing three calculations of Q at closely spaced intervals in β.[78,79] In particular, following the recommendation of Yamamoto,[78] for each Feynman path, we also calculate results for paths for which the deviation from the centroid position is scaled by $\sqrt{(\beta \pm \Delta\beta)/\beta}$, where $\Delta\beta$ is the finite difference step size. In the present set of calculations, we choose $\Delta\beta$ such that the higher temperature in the two finite difference calculations is 1% higher than the T value for which we are calculating the data; this choice yields good agreement with results calculated using 5-point finite differences. The thermodynamic functions are presented in Table IV. The following expressions were used to calculate the standard-state molar enthalpies and constant-pressure heat capacities:

$$H^\circ = \langle E \rangle + pV = \langle E \rangle + RT \tag{47}$$

and

$$C_P^\circ = C_V + R, \tag{48}$$

where p is the pressure, V is the volume, and R is the gas constant.

IV. RESULTS AND DISCUSSION

A. Numerical considerations

The calculations involve four computationally intensive steps: the selection of configuration space sample points (including energy evaluations used in the sampling), generating a random Feynman path from a free-particle distribution, evaluating the potential at points along the path, and the possible calculation of a numerical Hessian if the HGVR scheme is employed. Generating the Feynman path involves the calculation of $N \times P$ Gaussian random numbers and $O(N \times P)$ floating point operations by the sequential sectioning scheme[48] to generate the coordinates of the quadrature nodes and is typically no more than a few percent of the overall cost; however, any of the three other steps can be the dominant computational expense depending on the temperature and the choice of numerical parameters.

The costs associated with the selection of configuration space sample points and the calculation of Hessians (if using the HGVR scheme) can be ameliorated by calculating multiple paths for each accepted centroid configuration. These paths are highly correlated so whenever we do this we immediately

average the results of all paths for a given centroid configuration so that we can continue to use our uncertainty estimators that assume uncorrelated sampling. Sampling multiple paths per centroid configuration is less effective than uncorrelated sampling in terms of variance reduction, so this must be carefully weighed against the cost reductions. Moreover, such sampling reduces the effectiveness of the HGVR scheme, which works by correcting for the variance associated with the sum over paths for a given centroid with a harmonic-type treatment. At 300 and 400 K, we can sample many paths per centroid without markedly degrading variance reduction, but 10 paths per centroid are sufficient to ensure that the computational cost is dominated by the path integration. In Table V we consider for $T = 500$ K the effectiveness of sampling multiple paths per centroid, both with and without employing the HGVR scheme. We do this by comparing sampling variances rather than statistical uncertainties because the variances are proportional to the number of samples needed to achieve a given level of accuracy. If we do not use the HGVR scheme, even sampling 20 paths per centroid is observed to be about 73% as effective at variance reduction as fully independent samples. However, if we employ the HGVR scheme, which leads to a variance reduction of a factor of 14 at 500 K if one path per centroid is sampled, the effectiveness of additional samples per centroid is greatly reduced. For example, when using HGVR, the incremental variance reductions from adding a third, fourth, or fifth path for a given centroid (here we are considering the effect of adding one path to the previous set, i.e., three vs. two, four vs. three, and five vs. four) are only 44%, 41%, and 18% as effective, respectively, as incremental additions of fully independent samples. Thus, at $T = 500$ K, we opt to only sample four paths per centroid configuration.

In Table VI we consider the effectiveness of the HGVR scheme as a function of temperature when we sample only 1 path per centroid. We also tabulate the ratio of the relative variance, i.e., the absolute variance divided by the partition function squared, of a QM calculation to that of a classical calculation. The HGVR scheme achieves more than an order of magnitude of variance reduction in the 400–600 K temperature range but the benefits gradually decrease with increasing T because the average over paths becomes less demanding as the system begins to behave more classically. For $T = 600$ K, if we employ the HGVR scheme, the relative sampling variance is only about 3.6 times that of a classical calculation; thus, at this and higher temperatures, there is almost nothing to be gained from sampling more than one path per centroid. At 2000 K even without the HGVR scheme, the relative sampling variance is only about 1.5 times larger than in a classical simulation and the benefits of the HGVR scheme no longer outweigh the costs of the Hessian calculation. At 300 K, we see a substantial reduction in the effectiveness of the HGVR scheme compared to $T = 400$–600 K, apparently because anharmonicity becomes increasingly important for paths that meander far from the centroid configuration.

TABLE I. Parameters used in the path integral calculations.

Parameters	Notes	300 K	400 K	500 K	600 K
No. of centroid samples	...	2×10^9	2×10^7	2×10^7	2×10^7
No. of paths per centroid	...	10	10	4	1
Bounds for y_i^{M} (a_0); i = 1–4	...	1–4	1–4	1–4	1–4
Δ_i (a_0); $i = 1-4$	a	0.1	0.12	0.15	0.15
$y_{1,0}^{\mathrm{M}}$ (a_0)	a	2.067 29	2.067 29	2.067 29	2.067 29
$y_{2,0}^{\mathrm{M}}$ (a_0)	a	2.126 05	2.126 05	2.126 05	2.126 05
$y_{3,0}^{\mathrm{M}}$ (a_0)	a	2.170 92	2.170 92	2.170 92	2.170 92
$y_{4,0}^{\mathrm{M}}$ (a_0)	a	2.205 97	2.205 97	2.205 97	2.205 97
Δ_{θ_i} (deg); $i = 1-3$	a	10	10	10	10
$\theta_{0,1}$ (deg)	a	113.554	113.554	113.554	113.554
$\theta_{0,2}$ (deg)	a	109.007	109.007	109.007	109.007
$\theta_{0,3}$ (deg)	a	105.77	105.77	105.77	105.77
p_1^{tor}	a	0.75	0.75	0.75	0.75
p_2^{tor}	a	0.75	0.75	0.75	0.75
$\Delta_{\tau_1}^{(i)} i = 1-2$ (deg)	a	30	40	40	40
$\Delta_{\tau_2}^{(i)} i = 1-2$ (deg)	a	30	40	40	40
$\tau_{0,1}^{(i)} i = 1-2$ (deg)	a	±55.321	±55.321	±55.321	±55.321
$\tau_{0,2}^{(i)} i = 1-2$ (deg)	a	±64.793	±64.793	±64.793	±64.793
$N_{\text{geo-strata}}$	b	6	4	4	4
$R_{\text{thresh}}^{\text{CH}}$	c	0.07	0.08	0.08	0.1
$\mathrm{R}_{\text{thresh}}^{\text{HH}}$	c	0.3	0.4	0.4	0.6
$R_{\text{sec-thresh}}^{\text{CH}}$	c	0.05	n/a	n/a	n/a
$R_{\text{sec-thresh}}^{\text{HH}}$	c	0.2	n/a	n/a	n/a
N_{strata}	d	26	26	26	30
$\Delta E_{\text{main}}^{\text{strata}}$ (kcal/mol)	e	0.5	0.5	0.5	0.5
$\Delta E_{\text{first}}^{\text{strata}}$ (kcal/mol)	f	1	1	1.5	1.5
HGVR used?	...	Yes	Yes	Yes	Yes

TABLE I. (*Continued.*)

	Notes	700 K	800 K	900 K	1000 K
No. of centroid samples	...	1×10^7	1×10^7	1×10^7	1×10^7
No. of paths per centroid	...	1	1	1	1
Bounds for y_i^{M} (a_0); $i = 1-4$	...	1–4	1–4	1–4	1–4
Δ_i (a_0); $i = 1-4$	a	0.15	0.15	0.15	0.175
$y_{1,0}^{\mathrm{M}}$ (a_0)	a	2.067 29	2.067 29	2.067 29	2.067 29
$y_{2,0}^{\mathrm{M}}$ (a_0)	a	2.126 05	2.126 05	2.126 05	2.126 05
$y_{3,0}^{\mathrm{M}}$ (a_0)	a	2.170 92	2.170 92	2.170 92	2.170 92
$y_{4,0}^{\mathrm{M}}$ (a_0)	a	2.205 97	2.205 97	2.205 97	2.205 97
Δ_{θ_i} (deg); $i = 1-3$	a	10	12	12	12
$\theta_{0,1}$ (deg)	a	113.554	113.554	113.554	113.554
$\theta_{0,2}$ (deg)	a	109.007	109.007	109.007	109.007
$\theta_{0,3}$ (deg)	a	105.77	105.77	105.77	105.77
p_1^{tor}	a	0.75	0.75	0.75	0.75
p_2^{tor}	a	0.75	0.75	0.75	0.75
$\Delta_{\tau_1}^{(i)} i = 1-2$ (deg)	a	40	50	50	60
$\Delta_{\tau_2}^{(i)} i = 1-2$ (deg)	a	40	50	50	60
$\tau_{0,1}^{(i)} i = 1-2$ (deg)	a	±55.321	±55.321	±55.321	±55.321
$\tau_{0,2}^{(i)} i = 1-2$ (deg)	a	±64.793	±64.793	±64.793	±64.793
$N_{\text{geo-strata}}$	b	4	4	4	1
$R_{\text{thresh}}^{\text{CH}}$	c	0.12	0.15	0.18	n/a
$\mathrm{R}_{\text{thresh}}^{\text{HH}}$	c	0.7	0.8	0.9	n/a
$R_{\text{sec-thresh}}^{\text{CH}}$	c	n/a	n/a	n/a	n/a
$R_{\text{sec-thresh}}^{\text{HH}}$	c	n/a	n/a	n/a	n/a
N_{strata}	d	40	40	50	40
$\Delta E_{\text{main}}^{\text{strata}}$ (kcal/mol)	e	0.5	0.5	0.5	1
$\Delta E_{\text{first}}^{\text{strata}}$ (kcal/mol)	f	1.5	2	2	2
HGVR used?	...	Yes	Yes	Yes	Yes

	Notes	1200 K	1500 K	2000 K	2500 K
No. centroid samples	...	1×10^7	1×10^7	1×10^7	1×10^7
No. paths per centroid	...	1	1	1	1
Bounds for y_i^{M} (a_0); $i = 1-4$	...	1–4	1–4	1–4	1–4
Δ_i (a_0); $i = 1-4$	a	0.175	0.20	0.25	0.25
$y_{1,0}^{\mathrm{M}}$ (a_0)	a	2.067 29	2.067 29	2.067 29	2.067 29
$y_{2,0}^{\mathrm{M}}$ (a_0)	a	2.126 05	2.126 05	2.126 05	2.126 05
$y_{3,0}^{\mathrm{M}}$ (a_0)	a	2.170 92	2.170 92	2.170 92	2.170 92
$y_{4,0}^{\mathrm{M}}$ (a_0)	a	2.205 97	2.205 97	2.205 97	2.205 97
Δ_{θ_i} (deg); $i = 1-3$	a	12	15	20	20
$\theta_{0,1}$ (deg)	a	113.554	113.554	113.554	113.554
$\theta_{0,2}$ (deg)	a	109.007	109.007	109.007	109.007
$\theta_{0,3}$ (deg)	a	105.77	105.77	105.77	105.77
p_1^{tor}	a	0.75	0.75	0.75	0.75
p_2^{tor}	a	0.75	0.75	0.75	0.75
$\Delta_{\tau_1}^{(i)} i = 1-2$ (deg)	a	60	70	70	70
$\Delta_{\tau_2}^{(i)} i = 1-2$ (deg)	a	60	70	70	70
$\tau_{0,1}^{(i)} i = 1-2$ (deg)	a	±55.321	±55.321	±55.321	±55.321
$\tau_{0,2}^{(i)} i = 1-2$ (deg)	a	±64.793	±64.793	±64.793	±64.793
$N_{\text{geo-strata}}$	b	1	1	0	0
$R_{\text{thresh}}^{\text{CH}}$	c	n/a	n/a	n/a	n/a
$\mathrm{R}_{\text{thresh}}^{\text{HH}}$	c	n/a	n/a	n/a	n/a
$R_{\text{sec-thresh}}^{\text{CH}}$	c	n/a	n/a	n/a	n/a
$R_{\text{sec-thresh}}^{\text{HH}}$	c	n/a	n/a	n/a	n/a
N_{strata}	d	40	40	40	50
$\Delta E_{\text{main}}^{\text{strata}}$ (kcal/mol)	e	1	2	2	2
$\Delta E_{\text{first}}^{\text{strata}}$ (kcal/mol)	f	2	4	4	5
HGVR used?	...	Yes	Yes	No	No

TABLE I. (*Continued.*)

	Notes	3000 K
No. of centroid samples	...	1×10^7
No. of paths per centroid	...	1
Bounds for y_i^{M} (a_0); $i = 1-4$	...	1–4
Δ_i (a_0); $i = 1-4$	[a]	0.40
$y_{1,0}^{\mathrm{M}}$ (a_0)	[a]	2.067 29
$y_{2,0}^{\mathrm{M}}$ (a_0)	[a]	2.126 05
$y_{3,0}^{\mathrm{M}}$ (a_0)	[a]	2.170 92
$y_{4,0}^{\mathrm{M}}$ (a_0)	[a]	2.205 97
Δ_{θ_i} (deg); $i = 1-3$	[a]	25
$\theta_{0,1}$ (deg)	[a]	113.554
$\theta_{0,2}$ (deg)	[a]	109.007
$\theta_{0,3}$ (deg)	[a]	105.77
p_1^{tor}	[a]	0.75
p_2^{tor}	[a]	0.75
$\Delta_{\tau_1}^{(i)} i = 1-2$ (deg)	[a]	70
$\Delta_{\tau_2}^{(i)} i = 1-2$ (deg)	[a]	70
$\tau_{0,1}^{(i)} i = 1-2$ (deg)	[a]	±55.321
$\tau_{0,2}^{(i)} i = 1-2$ (deg)	[a]	±64.793
$N_{\text{geo-strata}}$	[b]	0
$R_{\text{thresh}}^{\text{CH}}$	[c]	n/a
$\mathrm{R}_{\text{thresh}}^{\text{HH}}$	[c]	n/a
$R_{\text{sec-thresh}}^{\text{CH}}$	[c]	n/a
$R_{\text{sec-thresh}}^{\text{HH}}$	[c]	n/a
N_{strata}	[d]	50
$\Delta E_{\text{main}}^{\text{strata}}$ (kcal/mol)	[e]	2
$\Delta E_{\text{first}}^{\text{strata}}$ (kcal/mol)	[f]	10
HGVR used?	...	No

[a] See Sec. II B for definitions of the importance function parameters.
[b] The number of geometry-defined strata.
[c] See Sec. IV A for definitions of the geometry-defined strata parameters.
[d] The total number of strata, including geometry-defined and energetically defined ones.
[e] The energy width of all energetically defined strata except the first and the last.
[f] The energy width of the first energetically defined stratum.

When using the HGVR scheme, we have found it useful to introduce an additional parameter to avoid numerical instabilities, namely, an upper bound on the norm of the gradient, which we set to 1 E_h; whenever the gradient exceeds this value, we omit the HGVR correction. The gradient term in the harmonic approximation of the reference potential has a zero contribution to the HGVR correction for the result with $P = P_{\max}$, but has a nonzero contribution for $P < P_{\max}$ because the reference potential expansion point may be slightly displaced from the centroid configuration of the lower-P paths. This parameter is only exceeded for a few very-high-energy configurations that should have a negligible contribution to the partition function at reasonable temperatures.

Except at low T, the most expensive component of our calculations is the cost of sampling appropriate centroid configurations, and we will discuss numerical considerations relating to this aspect of the algorithm next. Our sampling domain is specified by upper and lower bounds on the magnitudes of the GJ three-vectors $\mathbf{y}_i$; because our importance functions very effectively limit sampling of configurations having an unreasonable GJ vector magnitude, there is little to be gained from carefully optimizing these bounds so we simply choose very conservative values. We lightly optimize the parameters of our importance-sampling scheme to minimize the statistical uncertainty per unit of computer time; note carefully that this is different from choosing parameters to minimize the sampling variance because the parameters that minimize the variance may lead to a greater number of candidate samples being required in the stratification phase, which relies on expensive rejection sampling.

Our importance-sampling scheme has been discussed in detail previously;[45] the one new detail is the introduction of importance sampling in the dihedral degrees of freedom, as discussed in Sec. II. The benefit of importance sampling in the dihedral degrees of freedom is fairly modest; at 500 K, treating these two degrees of freedom reduces the sampling variance by a factor of about 1.4, although it also has the benefit of reducing the number of candidate samples needed for the stratification scheme by about a factor of 9.8.

For the present set of calculations, we use 0, 1, 4, or 6 geometry-defined strata depending on the temperature, with the largest number used at low T. The first such stratum

TABLE II. CH_4 partition functions, $Q^{[P]}(T)$, as a function of P and for $P \to \infty$ extrapolation values. Numbers in parentheses indicate 2σ statistical uncertainties in the last digits. The data include a factor of 16 to account for the effects of nuclear spin.

T (K)	300	400	500	600
P^{max}	96	72	48	36
$Q^{[P^{max}/6]}$	$5.0704(33) \times 10^{-17}$	$4.7483(31) \times 10^{-12}$	$6.5071(25) \times 10^{-9}$	$8.5152(32) \times 10^{-7}$
$Q^{[P^{max}/4]}$	$3.0157(20) \times 10^{-17}$	$3.2181(21) \times 10^{-12}$	$4.2454(17) \times 10^{-9}$	$5.5626(21) \times 10^{-7}$
$Q^{[P^{max}/3]}$	$2.4843(17) \times 10^{-17}$	$2.7837(19) \times 10^{-12}$	$3.6081(15) \times 10^{-9}$	$4.7185(18) \times 10^{-7}$
$Q^{[P^{max}/2]}$	$2.1541(15) \times 10^{-17}$	$2.5017(17) \times 10^{-12}$	$3.1965(13) \times 10^{-9}$	$4.1694(17) \times 10^{-7}$
$Q^{[P^{max}]}$	$1.9737(14) \times 10^{-17}$	$2.3432(16) \times 10^{-12}$	$2.9658(13) \times 10^{-9}$	$3.8607(16) \times 10^{-7}$
Extrapolation				
3 point #1[a]	$1.9195(16) \times 10^{-17}$	$2.2930(18) \times 10^{-12}$	$2.8933(14) \times 10^{-9}$	$3.7624(17) \times 10^{-7}$
3 point #2[b]	$1.9166(14) \times 10^{-17}$	$2.2922(16) \times 10^{-12}$	$2.8917(12) \times 10^{-9}$	$3.7613(15) \times 10^{-7}$
4 point #1[c]	$1.9165(18) \times 10^{-17}$	$2.2919(19) \times 10^{-12}$	$2.8917(15) \times 10^{-9}$	$3.7606(19) \times 10^{-7}$
4 point #2[d]	$1.9164(14) \times 10^{-17}$	$2.2922(16) \times 10^{-12}$	$2.8916(12) \times 10^{-9}$	$3.7613(15) \times 10^{-7}$
T (K)	700	800	900	1000
P^{max}	24	24	24	24
$Q^{[P^{max}/6]}$	$3.949\,37(168) \times 10^{-5}$	$4.552\,00(167) \times 10^{-4}$	$3.432\,54(135) \times 10^{-3}$	$1.895\,19(64) \times 10^{-2}$
$Q^{[P^{max}/4]}$	$2.286\,37(96) \times 10^{-5}$	$3.071\,25(119) \times 10^{-4}$	$2.560\,65(105) \times 10^{-3}$	$1.514\,16(53) \times 10^{-2}$
$Q^{[P^{max}/3]}$	$1.833\,54(79) \times 10^{-5}$	$2.631\,07(105) \times 10^{-4}$	$2.287\,31(96) \times 10^{-3}$	$1.390\,61(50) \times 10^{-2}$
$Q^{[P^{max}/2]}$	$1.546\,84(69) \times 10^{-5}$	$2.339\,72(96) \times 10^{-4}$	$2.101\,52(90) \times 10^{-3}$	$1.305\,30(47) \times 10^{-2}$
$Q^{[P^{max}]}$	$1.388\,47(63) \times 10^{-5}$	$2.173\,64(90) \times 10^{-4}$	$1.993\,76(86) \times 10^{-3}$	$1.255\,26(46) \times 10^{-2}$
Extrapolation				
3 point #1[a]	$1.339\,54(73) \times 10^{-5}$	$2.120\,47(94) \times 10^{-4}$	$1.958\,56(87) \times 10^{-3}$	$1.238\,81(46) \times 10^{-2}$
3 point #2[b]	$1.337\,95(62) \times 10^{-5}$	$2.119\,74(89) \times 10^{-4}$	$1.958\,46(85) \times 10^{-3}$	$1.238\,78(45) \times 10^{-2}$
4 point #1[c]	$1.338\,26(82) \times 10^{-5}$	$2.119\,95(98) \times 10^{-4}$	$1.958\,36(85) \times 10^{-3}$	$1.238\,75(46) \times 10^{-2}$
4 point #2[d]	$1.337\,84(62) \times 10^{-5}$	$2.119\,69(89) \times 10^{-4}$	$1.958\,45(85) \times 10^{-3}$	$1.238\,78(45) \times 10^{-2}$
T (K)	1200	1500	2000	2500
P^{max}	12	12	12	12
$Q^{[P^{max}/6]}$	$5.6049(22) \times 10^{-1}$	9.9588(37)	$3.4186(14) \times 10^{+2}$	$4.8832(27) \times 10^{+3}$
$Q^{[P^{max}/4]}$	$3.6142(15) \times 10^{-1}$	7.6025(29)	$2.9698(12) \times 10^{+2}$	$4.4863(25) \times 10^{+3}$
$Q^{[P^{max}/3]}$	$3.0169(12) \times 10^{-1}$	6.8383(27)	$2.8167(11) \times 10^{+2}$	$4.3490(24) \times 10^{+3}$
$Q^{[P^{max}/2]}$	$2.6193(11) \times 10^{-1}$	6.3098(25)	$2.7087(11) \times 10^{+2}$	$4.2513(23) \times 10^{+3}$
$Q^{[P^{max}]}$	$2.3918(10) \times 10^{-1}$	5.9991(24)	$2.6443(11) \times 10^{+2}$	$4.1928(23) \times 10^{+3}$
Extrapolation				
3 point #1[a]	$2.3188(10) \times 10^{-1}$	5.8974(24)	$2.6232(11) \times 10^{+2}$	$4.1734(23) \times 10^{+3}$
3 point #2[b]	$2.3177(10) \times 10^{-1}$	5.8966(24)	$2.6228(10) \times 10^{+2}$	$4.1733(23) \times 10^{+3}$
4 point #1[c]	$2.3180(10) \times 10^{-1}$	5.8968(24)	$2.6232(11) \times 10^{+2}$	$4.1733(24) \times 10^{+3}$
4 point #2[d]	$2.3177(10) \times 10^{-1}$	5.8965(24)	$2.6228(10) \times 10^{+2}$	$4.1732(23) \times 10^{+3}$
T (K)	3000			
P^{max}	12			
$Q^{[P^{max}/6]}$	$4.1985(24) \times 10^{+4}$			
$Q^{[P^{max}/4]}$	$3.9711(23) \times 10^{+4}$			
$Q^{[P^{max}/3]}$	$3.8917(23) \times 10^{+4}$			
$Q^{[P^{max}/2]}$	$3.8352(22) \times 10^{+4}$			
$Q^{[P^{max}]}$	$3.8013(22) \times 10^{+4}$			
Extrapolation				
3 point #1[a]	$3.7901(22) \times 10^{+4}$			
3 point #2[b]	$3.7900(22) \times 10^{+4}$			
4 point #1[c]	$3.7901(22) \times 10^{+4}$			
4 point #2[d]	$3.7900(22) \times 10^{+4}$			

[a]Extrapolation obtained with data for $P^{max}/4$, $P^{max}/3$, and $P^{max}/2$.
[b]Extrapolation obtained with data for $P^{max}/3$, $P^{max}/2$, and P^{max}.
[c]Extrapolation obtained with data for $P^{max}/6$, $P^{max}/4$, $P^{max}/3$, and $P^{max}/2$.
[d]Extrapolation obtained with data for $P^{max}/4$, $P^{max}/3$, $P^{max}/2$, and P^{max}.

includes all configurations where the two GJ dihedral angles are of the same sign, which happens 50% of the time. These are all fairly high-energy configurations that our importance function cannot discriminate against because it is restricted (for reasons of sampling efficiency) to be a product of one-dimensional functions and thus cannot account for correlations between two or more coordinates. If we employ more than one geometry-based stratum, the remaining such strata are defined

TABLE III. Comparison of CH_4 partition functions obtained by path integral calculations to those obtained[a] by VCI. Numbers in parentheses indicate 2σ statistical uncertainties in the last digits. The data include a factor of 16 to account for the effects of nuclear spin.

T (K)	Q (classical)	Q (path integral)	Q(VCI)[a]	Q(VCI)/Q (path integral)
300	$1.036\,81(2) \times 10^{-6}$	$1.916(1) \times 10^{-17}$	1.93×10^{-17}	1.007
400	$2.158\,3(3) \times 10^{-5}$	$2.292(2) \times 10^{-12}$	2.30×10^{-12}	1.003
500	$2.283\,2(4) \times 10^{-4}$	$2.892(1) \times 10^{-9}$	2.89×10^{-9}	0.999
600	$1.573\,3(3) \times 10^{-3}$	$3.761(2) \times 10^{-7}$	3.76×10^{-7}	1.000
700	$8.063(2) \times 10^{-3}$	$1.337\,8(6) \times 10^{-5}$	1.33×10^{-5}	0.994
800	$3.330\,3(9) \times 10^{-2}$	$2.119\,7(9) \times 10^{-4}$	2.11×10^{-4}	0.995
900	$1.166\,8(4) \times 10^{-1}$	$1.958\,5(9) \times 10^{-3}$	1.93×10^{-3}	0.985
1000	$3.585(1) \times 10^{-1}$	$1.238\,8(5) \times 10^{-2}$	1.22×10^{-2}	0.985
1200	2.516 3(9)	$2.318(1) \times 10^{-1}$	n/a	n/a
1500	$2.763(1) \times 10^{+1}$	5.897(2)	n/a	n/a
2000	$6.230(2) \times 10^{+2}$	$2.623(1) \times 10^{+2}$	n/a	n/a
2500	$7.188(4) \times 10^{+3}$	$4.173(2) \times 10^{+3}$	n/a	n/a
3000	$5.474(3) \times 10^{+4}$	$3.790(2) \times 10^{+4}$	n/a	n/a

[a]Chakraborty *et al.*[2]

based on two configuration properties

$$R_{\mathrm{dev}}^{\mathrm{CH}} = \sqrt{\sum_{i=1}^{4} \left(R(CH_i) - 2.0673\, a_0\right)^2} \tag{49}$$

and

$$R_{\mathrm{dev}}^{\mathrm{HH}} = \sqrt{\sum_{ij,i<j} \left(R(H_iH_j) - 3.375937493\, a_0\right)^2}, \tag{50}$$

where the numerical values are those of the associated atom-atom distances at the equilibrium configuration. In particular, we input two threshold parameters, $R_{\mathrm{thresh}}^{\mathrm{CH}}$ and $R_{\mathrm{thresh}}^{\mathrm{HH}}$, and configurations that do not fall into the first stratum (based on the torsional angles) fall into stratum #2 if $R_{\mathrm{dev}}^{\mathrm{CH}} > R_{\mathrm{thresh}}^{\mathrm{CH}}$ and $R_{\mathrm{dev}}^{\mathrm{HH}} > \mathrm{R}_{\mathrm{thresh}}^{\mathrm{HH}}$. Stratum #3 consists of samples for which $R_{\mathrm{dev}}^{\mathrm{CH}} > R_{\mathrm{thresh}}^{\mathrm{CH}}$ but $R_{\mathrm{dev}}^{\mathrm{HH}} < \mathrm{R}_{\mathrm{thresh}}^{\mathrm{HH}}$, and stratum #4 consists of samples for which $R_{\mathrm{dev}}^{\mathrm{HH}} > \mathrm{R}_{\mathrm{thresh}}^{\mathrm{HH}}$ but $R_{\mathrm{dev}}^{\mathrm{CH}} < R_{\mathrm{thresh}}^{\mathrm{CH}}$. These four strata are all primarily populated by high-energy configurations, so most candidate samples that fall within them are rejected before we need to calculate any energies for them. However, the *relative* sampling variance, i.e., the variance divided by the square of their contribution to Q, of these strata is relatively high compared to what would be achieved by energy stratification because energy stratification does a better job, especially at high-T, of sorting configurations into groups with similar contributions. At $T \geq 2000$ K, we employ no geometry-defined strata, and for $T \geq 1000$ K, we only employ the stratum defined by the torsion angles. At the lowest temperature considered, 300 K, which took about 98% of all the computer time for the calculations presented in Table II, we employed two additional geometry-defined strata, specified by two additional input parameters $R_{\mathrm{sec-thresh}}^{\mathrm{CH}}$ and $R_{\mathrm{sec-thresh}}^{\mathrm{HH}}$. Stratum #5 then consists of all configurations not already assigned to a prior stratum such that $R_{\mathrm{dev}}^{\mathrm{CH}} > R_{\mathrm{sec-thresh}}^{\mathrm{CH}}$, and stratum #6 consisted of all configurations not already assigned to strata 1–5

TABLE IV. Vibrational–rotational–translational standard state (1 bar) thermodynamic functions and differences between various theoretical heat capacity estimates as a function of temperature (T).[a]

T (K)	A°[b] (kJ/mol)	H° (kJ/mol)	S° (J mol^{-1} K^{-1})	C_P° (J mol^{-1} K^{-1})	ΔC_P°[c] (J mol^{-1} K^{-1})	ΔC_P°[d] (J mol^{-1} K^{-1})
300	63.596(2)	122.13	186.79	36.0	−0.2	0.05
400	43.516(2)	125.98	197.85	41.8	−1.2	0.13
500	22.393(2)	130.44	207.77	47.8	−1.2	0.29
600	0.315(2)	135.53	217.04	54.0	−1.2	0.51
700	−22.662(3)	141.23	225.82	59.9	−1.3	0.81
800	−46.496(3)	147.50	234.18	65.4	−1.4	1.15
900	−71.148(3)	154.28	242.16	70.5	−1.3	1.54
1000	−96.584(3)	161.56	249.83	75.0	−1.2	1.96
1200	−149.675(4)	177.35	264.21	82.7	−1.0	2.85
1500	−234.412(5)	203.59	283.69	91.7	−0.9	4.30
2000	−387.607(7)	252.22	311.60	102.1	−0.9	6.84
2500	−553.62(1)	305.29	335.25	109.7	−1.5	9.46
3000	−730.74(1)	362.60	356.13	118.6	−5.0	12.16

[a]The results do not include contributions from nuclear spin factors (see text).
[b]The Helmholtz free energy; the numbers in parentheses are 2σ statistical uncertainties in the last digits.
[c]The differences between the data of Gurvich *et al.*[85] and the path integral values for C_P° at 1 bar.
[d]The differences between the data of Gurvich *et al.*[85] and the values listed in the NIST–JANAF tables[86] for C_P° at 1 bar.

TABLE V. Comparison of statistical sampling variances (both with and without use of the HGVR scheme) for CH_4 partition functions at $T = 500$ K as the number of paths calculated per centroid configuration, N^{ppc}, is varied. All values are relative to the case with $N^{ppc} = 1$ and where the HGVR scheme is used.

N^{ppc}	σ^2(HGVR)[a]	σ^2(sans HGVR)[b]	σ^2(sans HGVR)/σ^2(HGVR)[c]
1	1.000	14.09	14.09
2	0.567	7.14	12.58
3	0.454	4.96	10.92
4	0.383	3.83	10.00
5	0.358	3.07	8.58
10	0.288	1.68	5.85
15	0.241	1.24	5.13
20	0.229	0.96	4.19

[a]The sampling variance when the HGVR scheme is used.
[b]The sampling variance when the HGVR scheme is not used.
[c]The ratio of the sampling variance when the HGVR scheme is not used to the variance when the HGVR scheme is employed.

such that $R^{HH}_{dev} > R^{HH}_{sec-thresh}$. This was done in an attempt to isolate marginally contributing configurations from the negligibly contributing configurations (binned to strata 1–4) so as to reduce the sampling variance within these strata.

The percentage of the total work that is expended sampling appropriate centroid configurations varies strongly with the temperature. At $T = 300$ K, we examined about 810 candidate configurations for each accepted configuration during the stratification process. Of these candidate configurations, 94% (including 7% that lie within strata 5 and 6) was rejected based on geometric criteria, so only about 46 energy evaluations were required to obtain an accepted configuration. Considering that we evaluated 10 paths, each requiring 96 energy evaluations (or three times as many energy evaluations if we evaluate heat capacities), for each accepted centroid configuration, it is clear that the sampling phase is only a minor component of the overall cost at this temperature. At $T = 900$ K, we examined about 88 samples per accepted centroid configuration; 78% of these was rejected based on geometric criteria so we required about 19 energy evaluations to obtain an accepted centroid configuration. For this case, we calculate only 1 path per centroid configuration and used only 24 energies per path, so the sampling phase is of comparable cost to that of energy evaluations involved in the path integration at this temperature. The cost of the sampling stage is, however, well warranted: the sampling variance of a calculation without stratification is about a factor of 98 larger at 900 K than that reported in Table II (stratification is even more effective at lower T; for example, at 500 K, a calculation that does not employ stratification has a variance that is a factor of 247 times higher than a calculation that does).

We now consider the numerical integration along the Feynman paths; the principal way to contain this cost is to use a robust extrapolation scheme to keep the number of quadrature points, P_{max}, to a minimum. In Sec. II E, we showed that we could use high-order extrapolation schemes to improve the convergence of analytical finite-P results for the one-dimensional harmonic oscillator, and we noted that the ESP scheme allows us to perform similar extrapolations even for data possessing statistical uncertainty. In Fig. 2 we plot the absolute magnitude of the relative error in $Q^{[P]}$ vs. P_{max} for several extrapolation schemes at $T = 500$ K (the numerical parameters used for these calculations are the same as given in Table I except that we used $P_{max} = 288$ instead

TABLE VI. Comparison of the effectiveness of the HGVR scheme as a function of temperature for calculations of CH_4 partition functions. All calculations are for 1 path per centroid configuration.

T	No. HGVR to HGVR[a]	HGVR to classical[b]	No. HGVR to classical[c]
300	5.26	9350	49 200
400	12.6	160	2 010
500	14.1	13.4	188
600	12.8	3.57	45.7
700	9.55	2.32	22.2
800	6.52	2.23	14.5
900	4.15	1.87	7.73
1000	3.66	1.65	6.03
1200	2.13	1.37	2.93
1500	1.56	1.36	2.11
2000	1.23	1.22	1.50

[a]The ratio of the relative variance (the variance, i.e., σ^2, divided by Q^2) of $Q^{[P\max]}$ calculated without the HGVR scheme to the relative variance of $Q^{[P\max]}$ calculated with the HGVR scheme.
[b]The ratio of the relative variance of $Q^{[P\max]}$ calculated with the HGVR scheme to the relative variance of a classical ($P = 1$) calculation.
[c]The ratio of the relative variance of $Q^{[P\max]}$ calculated without the HGVR scheme to the relative variance of a classical ($P = 1$) calculation.

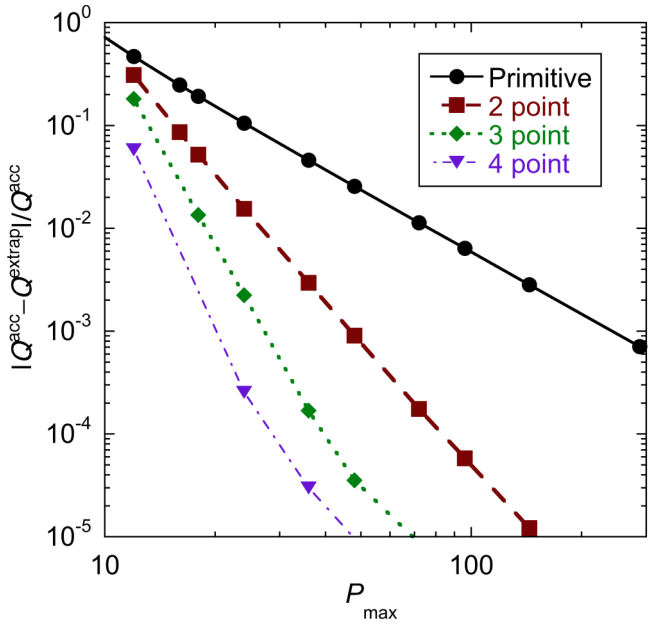

FIG. 2. A comparison of relative errors vs. P for primitive $Q^{[P]}$ calculations and various extrapolation schemes [Eqs. (33), (34), and (36)] for CH_4 at T = 500 K. The accurate result, Q^{acc}, is taken from a 5-point extrapolation using Eq. (39) with P_{max} = 288.

of 48); the most accurate result is estimated from a 5-point extrapolation using Eq. (39) with $P_{max} = 288$. The 2σ (two standard deviations) statistical uncertainty of the calculations is about 0.04%, and, as seen in this figure, the extrapolation uncertainty can be reduced to more than an order of magnitude below this statistical uncertainty. It is interesting to note that reducing the discretization error to below that of the statistical error would require $P_{max} \approx 400$ if one were relying on the primitive results but this can be achieved with $P_{max} \approx 60$, 36, or 24 if extrapolating with 2-point, 3-point, or 4-point formulas, respectively.

In the calculations presented in Table II, we restrict P_{max} to be divisible by 12 and tabulate data for P_{max}, $P_{max}/2$, $P_{max}/3$, $P_{max}/4$, and $P_{max}/6$. We evaluate two sets of 3-point extrapolated results [using Eqs. (34) and (41)] and two results of 4-point extrapolations [using Eqs. (36) and (42)]; one extrapolation result at each order takes advantage of the highest values of P and the second uses data sets for which the highest value of P is $P_{max}/2$. The difference between two such extrapolations at a given order provides a conservative estimate of the uncertainty in the estimated $P \to \infty$ limit. We observe good agreement between all the extrapolated results, although the agreement between the two 4-point results is better than that between the two 3-point results, which indicates that the $O(P^{-8})$ extrapolations, as expected, provide better accuracy than the lower-order formulas. We also observe that the agreement between the two 4-point extrapolations is typically much better than the statistical uncertainty, and because the second extrapolation is expected to be more than an order of magnitude more accurate than the first, this suggests that the extrapolation error of our best results is negligible compared to the statistical uncertainty.

Arguably, we might have achieved useful results using P_{max} values that are about a factor of 2 lower than those we adopted for the calculations in Table II. A number of factors motived us to use higher values though. First, we wished to demonstrate unambiguously that the extrapolation error could be reduced to more than an order of magnitude below the statistical uncertainty from the sampling by using a second set of extrapolated results relying on data only up to $P_{max}/2$. Second, the present calculations, except at low T, are dominated by sampling costs, so we would observe only modest savings from using lower P_{max} values. Third, there is an increase in the statistical uncertainty of the extrapolated data when we use lower values of P_{max}. An example of this effect is given in Table VII for methane partition functions at $T = 400$ K. There is an increase in the relative uncertainty, compared to that of the $Q^{[P_{max}]}$ calculation, for the extrapolated values, and this increases with increasing order of the extrapolations. This effect is quite modest for large values of P_{max} but becomes much more significant for smaller values of P_{max}. For example, with $P_{max} = 24$, we see that we can only achieve high accuracy with the 5- and 6-point extrapolations, but that these extrapolations increase the relative uncertainty compared to that of $Q^{[P_{max}]}$ by factors of 2.2 and 2.9, respectively. This effect limits the regime of usefulness of the higher-order extrapolation formulas.

As discussed in Sec. II E, Eq. (22) of the HGVR scheme is strictly valid only when the INM frequencies are evaluated at the centroid configuration; however, when using the ESP extrapolation approach, paths with $P < P_{max}$ have a centroid position that deviates slightly from the centroid of all P_{max} points, which is the configuration at which the reference potential is defined. In Table VIII we compare results at $T = 500$ K and $P_{max} = 48$ that use the HGVR scheme to those of two independent calculations done without the HGVR scheme, but with 10 times as many samples so as to obtain comparable uncertainties to the first set of results. The three different results for $P = 48$ only differ due to statistical uncertainties, but the differences for $P < 48$ are primarily due to errors from applying the HGVR correction with approximate centroids. At $P = 24$, this error is about 0.1% and it increases to about 1.2% at $P = 6$. However, there is little evidence of these errors affecting the accuracy of any of the extrapolated results that are tabulated using 3-, 4-, 5-, and 6-point formulas. In particular, we see that all 4 different extrapolation schemes yield essentially the same result even though the higher-order ones rely on data with increasing errors if the HGVR scheme is employed. Importantly, the extrapolated results for the two calculations that do not use the HGVR scheme do not differ significantly from the extrapolated results for the calculations that use the HGVR scheme.

B. Comparison of path integral and VCI results

Finally, we turn our attention to a comparison of the path integral benchmarks to the prior VCI calculations of Chakraborty *et al.* In order to obtain affordable results, those calculations were limited to a three-mode approximation in a modestly sized basis set. Unfortunately, two other factors limited the accuracy of these calculations.[80] First, the PES, as originally distributed, contained a coding error: the out-of-plane bend terms were intended to be evaluated only using a right-handed set of CH bond vectors but, depending on the input geometry, the code sometimes also evaluated this

TABLE VII. A comparison of the statistical uncertainty in extrapolated results as a function of P_{max} for methane partition functions at $T = 400$ K. Numbers in parentheses indicate 2σ statistical uncertainties in the last digits. The data include a factor of 16 to account for the effects of nuclear spin.

	$P_{max} = 24$	$P_{max} = 48$	$P_{max} = 72$
$Q^{[P\max/8]}$	$1.1358(290) \times 10^{-9}$	$2.5231(280) \times 10^{-11}$	$7.7735(52) \times 10^{-12}$
$Q^{[P\max/6]}$	$1.7460(64) \times 10^{-10}$	$1.0240(74) \times 10^{-11}$	$4.7483(31) \times 10^{-12}$
$Q^{[P\max/4]}$	$2.5268(30) \times 10^{-11}$	$4.7507(33) \times 10^{-12}$	$3.2181(21) \times 10^{-12}$
$Q^{[P\max/3]}$	$1.0245(87) \times 10^{-11}$	$3.5071(24) \times 10^{-12}$	$2.7837(19) \times 10^{-12}$
$Q^{[P\max/2]}$	$4.7513(36) \times 10^{-12}$	$2.7851(19) \times 10^{-12}$	$2.5017(17) \times 10^{-12}$
$Q^{[P\max]}$	$2.7862(21) \times 10^{-12}$	$2.4096(17) \times 10^{-12}$	$2.3432(16) \times 10^{-12}$
Extrapolated values			
3-point	$2.3530(23) \times 10^{-12}$	$2.2940(17) \times 10^{-12}$	$2.2922(16) \times 10^{-12}$
4-point	$2.2766(31) \times 10^{-12}$	$2.2932(17) \times 10^{-12}$	$2.2922(16) \times 10^{-12}$
5-point	$2.2982(38) \times 10^{-12}$	$2.2932(17) \times 10^{-12}$	$2.2922(16) \times 10^{-12}$
6-point	$2.2931(50) \times 10^{-12}$	$2.2931(17) \times 10^{-12}$	$2.2922(16) \times 10^{-12}$
Relative uncertainty ratio[a]			
3-point	1.309	1.025	1.008
4-point	1.804	1.040	1.011
5-point	2.200	1.052	1.013
6-point	2.891	1.062	1.014

[a]The ratio of the relative uncertainty (the uncertainty divided by the partition function) of the extrapolated results to the relative uncertainty for the calculation of $Q^{[P\max]}$.

expression using a left-handed set of vectors. This coding error resulted in the work of some groups being qualitatively incorrect; for example, Schiffel and Manthe[81] report that discrepancies between their results and those of the Zhang *et al.*[82] were due to Zhang *et al.* using the incorrectly coded PES. Fortunately, the coordinate system selected for the VCI calculations[2] resulted in nearly the entire quadrature grid using a right-handed set of vectors. The second complication was due to the fact that the incident H atom position in calls to the $H + CH_4$ potential was not displaced sufficiently far from the CH_4 group to obtain the accurate isolated-methane limit; this, for example, resulted in an error of about 3 cm^{-1} in the ground state eigenvalue. A corrected version of the JG PES may be obtained from the POTLIB online library of potential energy surfaces.[83,84]

We note that the present calculations include not only the spin symmetry factor discussed in Sec. III but also a permutational symmetry factor of $1/\sigma_{sym} = 1/(4!) = 1/24$ as explained in Sec. II, whereas the VCI calculations include not only the spin symmetry factor but also the rigid rotor symmetry factor of 1/12. The latter is appropriate for that calculation because the VCI calculation does not include configurations equivalent to permutations corresponding to an odd number of elementary transpositions of pairs of H atoms. Although these treatments differ in their treatment of symmetry, each is correct for the type of calculation involved, and so they may be compared without any further symmetry consideration.

The comparison of the present path integral results to the previous VCI ones is shown in Table III. Since the present

TABLE VIII. Comparison of $T = 500$ K CH_4 partition functions obtained with the HGVR scheme to those of two sets of calculations without the HGVR scheme.[a] Numbers in parentheses indicate 2σ statistical uncertainties in the last digits.

P	With HGVR	No. HGVR set 1	No. HGVR set 2	Ratio 1[b]	Ratio 2[c]
6	$1.099\ 98(45) \times 10^{-8}$	$1.113\ 14(50) \times 10^{-8}$	$1.113\ 20(50) \times 10^{-8}$	0.988 18	0.988 13
8	$6.507\ 1(25) \times 10^{-9}$	$6.554\ 0(27) \times 10^{-9}$	$6.554\ 1(27) \times 10^{-9}$	0.992 84	0.992 83
12	$4.245\ 4(17) \times 10^{-9}$	$4.260\ 7(18) \times 10^{-9}$	$4.260\ 6(18) \times 10^{-9}$	0.996 39	0.996 41
16	$3.608\ 1(15) \times 10^{-9}$	$3.615\ 4(15) \times 10^{-9}$	$3.615\ 8(15) \times 10^{-9}$	0.997 99	0.997 88
24	$3.196\ 5(13) \times 10^{-9}$	$3.199\ 6(14) \times 10^{-9}$	$3.199\ 7(14) \times 10^{-9}$	0.999 02	0.998 99
48	$2.965\ 8(13) \times 10^{-9}$	$2.966\ 6(13) \times 10^{-9}$	$2.966\ 8(13) \times 10^{-9}$	0.999 75	0.999 69
Extrapolation[d]					
3 point	$2.891\ 7(12) \times 10^{-9}$	$2.891\ 6(13) \times 10^{-9}$	$2.891\ 9(13) \times 10^{-9}$	1.000 01	0.999 92
4 point	$2.891\ 6(12) \times 10^{-9}$	$2.891\ 5(13) \times 10^{-9}$	$2.891\ 8(13) \times 10^{-9}$	1.000 03	0.999 92
5 point	$2.891\ 6(13) \times 10^{-9}$	$2.891\ 4(13) \times 10^{-9}$	$2.891\ 8(13) \times 10^{-9}$	1.000 04	0.999 92
6 point	$2.891\ 6(13) \times 10^{-9}$	$2.891\ 4(13) \times 10^{-9}$	$2.891\ 8(13) \times 10^{-9}$	1.000 05	0.999 92

[a]The calculations used the parameters in Table I except that the two calculations performed without the HGVR scheme used 10 times as many centroid samples.
[b]The ratio of the results obtained with the HGVR scheme to the set 1 results obtained without the HGVR scheme.
[c]The ratio of the results obtained with the HGVR scheme to the set 2 results obtained without the HGVR scheme.
[d]The n-point extrapolations use the data for the n highest values of P.

results are very well converged, this provides a test of the VCI calculations. We observe excellent agreement; the largest errors in the VCI calculations are −1.5% and occur at the highest temperature for which these results were tabulated. The agreement is clearly partially fortuitous because the error resulting from the failure to displace the incident H atom in the call to the $H + CH_4$ potential at the isolated methane limit was estimated to lead to a shift in the eigenvalues of -3 cm^{-1} and this would be expected to lower the partition function at 300 K by about 1.5% yet the VCI calculations are still 0.7% higher than the path integral calculations at this temperature. Nevertheless, the level of agreement observed is sufficient to lend confidence to the overall conclusions of the earlier work despite the errors relating to the incorrect implementation of the potential and the various approximations. It is a milestone in the field that converged partition functions for the same problem have now been obtained by two entirely different methods.

C. Thermodynamic functions

As mentioned in Sec. III, in addition to the partition functions, we also tabulate, in Table IV, the standard state values (at a pressure of 1 bar) of the Helmholtz free energy (A°), the enthalpy (H°), the entropy (S°), and the constant-pressure heat capacity (C_P°). Because the relative statistical uncertainty in ln Q is smaller than that in Q, the relative uncertainties in the vibrational–rotational contributions to A are typically smaller than those for the partition function. The relative uncertainties in S° and H° are also typically significantly smaller than those for Q; however, statistical uncertainties in the heat capacities are much larger than for the other quantities. Because S°, H°, and C_P° involve derivatives of ln Q, we do not directly obtain statistical uncertainty estimates for these quantities. However, for several temperatures, we have obtained estimates of the magnitude for these uncertainties by performing several independent calculations; these calculations suggest that the values listed in Table IV have a statistical uncertainty in only the final digit tabulated.

We also tabulate in Table IV the difference between C_P° at 1 bar obtained from the thermochemical tabulations of Gurvich *et al.*,[85] which include corrections for anharmonicity and vibrational–rotational coupling, and the path integral values; for comparison, we also list the difference between the data of Gurvich *et al.*[85] and the more-approximate theoretical results given in the NIST–JANAF tables,[86] which are calculated using a separable treatment of rotation and vibration and a harmonic treatment of vibration.[85] At low T, the JANAF heat capacities are in better agreement with the data of Gurvich *et al.*[85] than the path integral results, presumably because of inaccuracies in the JG PES; whereas at high T, the path integral results show better agreement with the data of Gurvich *et al.*,[85] presumably because anharmonic effects are more important at high T.

A single direct experimental determination of S°, 188.66 ± 0.42 J K^{-1} mol^{-1} at T = 298.15 K and 1 atm pressure, is available from the calorimetry measurements of Colwell *et al.*;[87] this corresponds to a value at 1 bar of 188.77 ± 0.42 J K^{-1} mol^{-1}. However, this value is generally viewed to be inaccurate; for example, Friend *et al.*,[88] in their comprehensive evaluation of experimental data on methane, recommend a value for S(298.15 K, 1 atm) of 186.27 J K^{-1} mol^{-1}, which would correspond to a value at 1 bar of S° (298.15 K) of 186.38 J K^{-1} mol^{-1}. This recommendation is in good agreement with the results in the NIST–JANAF tables of 186.25 ± 0.04 J K^{-1} mol^{-1}. By approximating C_P° as constant in the 298.15–300 K temperature range, we can obtain an estimate of S°(298.15 K) from our C_P° and S° data at 300 K by

$$S^\circ(298.15\ \mathrm{K}) = S^\circ(300\ \mathrm{K}) - \int_{298.15}^{300} dT C_P^\circ/T \approx S^\circ(300\ \mathrm{K}) - C_P^\circ(300\ \mathrm{K})\ \ln(300/298.15) \quad (51)$$

which yields a value of 186.57 J K^{-1} mol^{-1} that is in reasonable agreement with the recommendation of Friend *et al.*[88] and the value in the NIST–JANAF tables.

V. SUMMARY

We have presented three improvements to our path integral methods. The first is a generalization of our importance-sampling scheme to include sampling in dihedral angles. The second is an extension of our stratification strategy to permit some strata defined purely by geometric information whereas the most important strata are defined both by geometrical criteria and by the energy of the centroid configuration. This allows us to retain the outstanding variance reduction (typically the statistical uncertainty is reduced by one order of magnitude) of energy stratification while greatly reducing the cost of the associated energy evaluations. The third improvement is a revised scheme for extrapolating partition functions calculated with P path discretization points to the $P \to \infty$ limit, with improved convergence orders ranging from $O(P^{-6})$ to $O(P^{-12})$. We extrapolate on a path-by-path basis that allows us to obtain rigorous uncertainty estimates for the extrapolated quantities.

We used the new methods to calculate accurate path integral partition functions for CH_4 with the well-studied JG potential energy surface. These results are compared to previous results[2] obtained by VCI. The VCI calculations[2] are found to agree with our path integral benchmarks to within 1.5%. The partition functions presented here for methane are the most accurate partition functions reported for any molecule with more than four atoms on a known PES, and they could be used as benchmarks for testing other methods in the future.

Finally, we also calculated standard-state heat capacities, entropies, enthalpies, and free energies. We compared the calculated heat capacities to the anharmonically corrected experimentally based values in the thermodynamic tables of Gurvich *et al.*[85] and to the harmonic treatment in the NIST–JANAF tables. At high temperature, the present results agree better than the NIST–JANAF tables with the Gurvich *et al.* tabulations, but the accuracy is apparently lower at low temperature, presumably due to inaccuracies in the potential energy surface.

ACKNOWLEDGMENTS

This work was supported in part by the U.S. Department of Energy, Office of Basic Energy Sciences, under Grant No. DE-FG02-86ER13579.

[1]D. A. McQuarrie, *Statistical Mechanics* (Harper & Row, New York, 1973).
[2]A. Chakraborty, D. G. Truhlar, J. M. Bowman, and S. Carter, J. Chem. Phys. **121**, 2071 (2004).
[3]G. D. Carney, L. L. Sprandel, and C. W. Kern, Adv. Chem. Phys. **37**, 305 (1978).
[4]T. C. Thompson and D. G. Truhlar, Chem. Phys. Lett. **75**, 87 (1980).
[5]S. Carter and J. M. Bowman, J. Chem. Phys. **108**, 4397 (1998).
[6]S. Carter, J. M. Bowman, and N. C. Handy, Theor. Chem. Acc. **100**, 191 (1998).
[7]J. Wu, X. Huang, S. Carter, and J. M. Bowman, Chem. Phys. Lett. **426**, 285 (2006).
[8]R. J. Whitehead and N. C. Handy, J. Mol. Spectrosc. **55**, 356 (1975).
[9]S. Carter, S. J. Culik, and J. M. Bowman, J. Chem. Phys. **107**, 10458 (1997).
[10]P. N. Day and D. G. Truhlar, J. Chem. Phys. **95**, 6615 (1991).
[11]W. C. Necoechea and D. G. Truhlar, Chem. Phys. Lett. **224**, 297 (1994).
[12]S. Carter and J. M. Bowman, J. Phys. Chem. A **104**, 2355 (2000).
[13]M. Neff and G. Rauhut, J. Chem. Phys. **131**, 124129 (2009).
[14]S. L. Mielke, A. Chakraborty, and D. G. Truhlar, J. Phys. Chem. A **117**, 7327 (2013).
[15]A. Chakraborty and D. G. Truhlar, J. Chem. Phys. **124**, 184310 (2006).
[16]G. M. Chaban, J. O. Jung, and R. B. Gerber, J. Chem. Phys. **111**, 1823 (1999).
[17]M. J. T. Jordan and R. G. Gilbert, J. Chem. Phys. **102**, 5669 (1995).
[18]R. P. Feynman, *Statistical Mechanics* (Benjamin, Reading, 1972).
[19]R. P. Feynman and A. R. Hibbs, *Quantum Mechanics and Path Integrals* (McGraw-Hill, New York, 1965).
[20]H. Kleinert, *Path Integrals in Quantum Mechanics, Statistics, Polymer Physics, and Financial Markets*, 3rd ed. (World Scientific, Singapore, 2004).
[21]D. Ceperley, Rev. Mod. Phys. **67**, 279 (1995).
[22]B. J. Berne and D. Thirumalai, Annu. Rev. Phys. Chem. **37**, 401 (1986).
[23]J. D. Doll, D. L. Freeman, and T. L. Beck, Adv. Chem. Phys. **78**, 61 (1990).
[24]C. Chakravarty, Int. Rev. Phys. Chem. **16**, 421 (1997).
[25]K.-Y. Wong, Commun. Comput. Phys. **15**, 853 (2014).
[26]X.-G. Wang and T. Carrington, Jr., J. Chem. Phys. **119**, 101 (2003).
[27]X.-G. Wang and T. Carrington, Jr., J. Chem. Phys. **138**, 104106 (2013).
[28]E. Matyus, J. Simunek, and A. G. Csaszar, J. Chem. Phys. **131**, 074106 (2009).
[29]H.-G. Yu, J. Chem. Phys. **121**, 6334 (2004).
[30]D. W. Schwenke and H. Partridge, Spectrochim. Acta, Part A **57**, 887 (2001).
[31]F. Huarte-Larrañaga and U. Manthe, J. Chem. Phys. **113**, 5115 (2000).
[32]J. M. Bowman, D. Wang, X. Huang, F. Huarte-Larranaga, and U. Manthe, J. Chem. Phys. **114**, 9683 (2001).
[33]J. Pu, J. C. Corchado, and D. G. Truhlar, J. Chem. Phys. **115**, 6266 (2001).
[34]J. M. Bowman, Adv. Chem. Phys. **61**, 115 (1985).
[35]J. M. Bowman, Theor. Chem. Acc. **108**, 125 (2002).
[36]J. M. Bowman, J. Phys. Chem. **95**, 4960 (1991).
[37]S. L. Mielke, G. C. Lynch, D. G. Truhlar, and D. W. Schwenke, Chem. Phys. Lett. **216**, 441 (1993).
[38]S. L. Mielke, G. C. Lynch, D. G. Truhlar, and D. W. Schwenke, J. Phys. Chem. **98**, 8000 (1994).
[39]J. M. Bowman and A. F. Wagner, *The Theory of Chemical Reaction Dynamics*, edited by D. C. Clary (Reidel, Dordrect, 1986), p. 47.
[40]S. L. Mielke, J. Srinivasan, and D. G. Truhlar, J. Chem. Phys. **112**, 8758 (2000).
[41]J. Srinivasan, Y. L. Volobuev, S. L. Mielke, and D. G. Truhlar, Comput. Phys. Commun. **128**, 446 (2000).
[42]S. L. Mielke and D. G. Truhlar, J. Chem. Phys. **114**, 621 (2001).
[43]S. L. Mielke and D. G. Truhlar, J. Chem. Phys. **115**, 652 (2001).
[44]S. L. Mielke and D. G. Truhlar, Chem. Phys. Lett. **378**, 317 (2003).
[45]V. A. Lynch, S. L. Mielke, and D. G. Truhlar, J. Chem. Phys. **121**, 5148 (2004).
[46]V. A. Lynch, S. L. Mielke, and D. G. Truhlar, J. Phys. Chem. A **109**, 10092 (2005).
[47]K. E. Anderson, S. L. Mielke, J. I. Siepmann, and D. G. Truhlar, J. Phys. Chem. A **113**, 2053 (2009).
[48]S. L. Mielke and D. G. Truhlar, J. Phys. Chem. A **113**, 4817 (2009).
[49]S. L. Mielke and D. G. Truhlar, J. Chem. Theory Comput. **8**, 1589 (2012).
[50]S. L. Mielke, M. Dinpajooh, J. I. Siepmann, and D. G. Truhlar, J. Chem. Phys. **138**, 014110 (2013).
[51]D. W. Jepsen and J. O. Hirschfelder, Proc. Natl. Acad. Sci. U.S.A. **45**, 249 (1959).
[52]G. Marsaglia and W. W. Tsang, J. Stat. Software **5**(8), 1 (2000), available online at http://www.jstatsoft.org/v05/i08.
[53]J. E. Adams and R. M. Stratt, J. Chem. Phys. **93**, 1332 (1990).
[54]K. S. Schweizer, R. M. Stratt, D. Chandler, and P. G. Wolynes, J. Chem. Phys. **75**, 1347 (1981).
[55]R. Q. Topper and D. G. Truhlar, J. Chem. Phys. **97**, 3647 (1992).
[56]R. Q. Topper, Q. Zhang, Y.-P. Liu, and D. G. Truhlar, J. Chem. Phys. **98**, 4991 (1993).
[57]R. D. Coalson, J. Chem. Phys. **85**, 926 (1986).
[58]A. Cuccoli, A. Macchi, G. Pedrolli, V. Tognetti, and R. Vaia, Phys. Rev. B **51**, 12369 (1995).
[59]M. Suzuki, Phys. Lett. A **113**, 299 (1985).
[60]L. Brualla, K. Sakkos, J. Boronat, and J. Casulleras, J. Chem. Phys. **121**, 636 (2004).
[61]M. Suzuki, Phys. Rev. B **31**, 2957 (1985).
[62]R. P. Steele, J. Zwickl, P. Shushkov, and J. C. Tully, J. Chem. Phys. **134**, 074112 (2011).
[63]R. D. Coalson, D. L. Freeman, and J. D. Doll, J. Chem. Phys. **85**, 4567 (1986).
[64]J. D. Doll, R. D. Coalson, and D. L. Freeman, Phys. Rev. Lett. **55**, 1 (1986).
[65]C. Predescu, J. Math. Phys. **44**, 1226 (2003).
[66]C. Predescu, D. Sabo, and J. D. Doll, J. Chem. Phys. **119**, 4641 (2003).
[67]E. Curotto, J. Chem. Phys **123**, 134102 (2005).
[68]C. Predescu and J. D. Doll, J. Chem. Phys. **117**, 7448 (2002).
[69]C. Predescu and J. D. Doll, Phys. Rev. E **67**, 026124 (2003).
[70]C. Predescu, J. Phys. Chem. B **110**, 667 (2005).
[71]M. Takahashi and M. Imada, J. Phys. Soc. Jpn. **53**, 3765 (1984).
[72]X.-P. Li and J. Q. Broughton, J. Chem. Phys. **86**, 5094 (1987).
[73]M. Suzuka, Phys. Lett. A **180**, 232 (1993).
[74]S. D. Kunikeev, D. L. Freeman, and J. D. Doll, Phys. Rev. E **81**, 066707 (2010).
[75]R. E. Zillich, J. M. Mayrhofer, and S. A. Chin, J. Chem. Phys. **132**, 044103 (2010).
[76]A. Bogojević, A. Balaž, and A. Belić, Phys. Rev. Lett. **94**, 180403 (2005).
[77]E. B. Wilson, Jr., J. Chem. Phys. **3**, 276 (1935).
[78]T. M. Yamamoto, J. Chem. Phys. **123**, 104101 (2005).
[79]C. Predescu, D. Sabo, J. D. Doll, and D. L. Freeman, J. Chem. Phys. **119**, 12119 (2003).
[80]A. Chakraborty, D. G. Truhlar, J. M. Bowman, and S. Carter, J. Chem. Phys. **135**, 119904 (2011).
[81]G. Schiffel and U. Manthe, J. Chem. Phys. **132**, 184103 (2010).
[82]L. Zhang, Y. Lu, S.-Y. Lee, and D. H. Zhang, J. Chem. Phys. **127**, 234313 (2007).
[83]R. J. Duchovic, Y. L. Volobuev, G. C. Lynch, D. G. Truhlar, T. C. Allison, A. F. Wagner, B. C. Garrett, and J. C. Corchado, Comput. Phys. Commun. **144**, 169 (2002); **156**, 319 (2004).
[84]R. J. Duchovic, Y. L. Volobuev, G. C. Lynch, A. W. Jasper, K. R. Yang, D. G. Truhlar, T. C. Allison, A. F. Wagner, B. C. Garrett, J. Espinosa-García, and J. C. Corchado, POTLIB online at http://comp.chem.umn.edu/potlib. This internet site provides the currently updated version of the POTLIB library and allows downloading of any of the potential energy functions in the library.
[85]L. V. Gurvich, I. V. Veyts, and C. B. Alcock, *Thermodynamic Properties of Individual Substances*, 4th ed. (Hemisphere, New York, 1989).
[86]*NIST-JANAF Thermochemical Tables*, 4th ed., Journal of Physics and Chemistry Reference Data, Monograph 9, edited by M. W. Chase, Jr. (American Chemical Society/American Institute of Physics, 1998).
[87]J. H. Colwell, E. K. Gill, and J. A. Morrison, J. Chem. Phys. **39**, 635 (1963).
[88]D. G. Friend, J. F. Ely, and H. Ingham, J. Phys. Chem. Ref. Data **18**, 583 (1989).